Safety Regulation Group

CAA PAPER 2002/7

A Study into the Response of Aircraft Fuel Tanks to Rapid Decelerations

www.caa.co.uk

Safety Regulation Group

Civil Aviation Authority

CAA PAPER 2002/7

A Study into the Response of Aircraft Fuel Tanks to Rapid Decelerations

Report prepared by Structures and Materials Department

Important Note

The CAA has made many of the documents that it publishes available electronically (in addition to traditional printed format). Where practical, the opportunity has been taken to incorporate a clearer revised appearance to the documents. Any significant changes to the content of this document will be shown in the Explanatory Note. If no such changes are indicated the material contained in this document, although different in appearance to the previously printed version, is unchanged. Further information about these changes and the latest version of documents can be found at www.caa.co.uk.

November 2002

ISBN 0 86039 8315

Issued November 2002

Enquiries regarding the content of this publication should be addressed to:
Research Management Department, Safety Regulation Group, Civil Aviation Authority, Aviation House, Gatwick Airport South, West Sussex, RH6 0YR.

The latest version of this document is available in electronic format at www.caa.co.uk, where you may also register for e-mail notification of amendments.

Printed copies and amendment services are available from: Documedia Solutions Ltd., 37 Windsor Street, Cheltenham, Glos., GL52 2DG.

Abstract

Evidence from service experience indicates that transient decelerations arising from emergency landings have significantly exceeded the levels defined in the Joint Airworthiness Requirements without pressure induced failure of the fuel tanks. It has been suggested that this may be due to dynamic conditions being less damaging than the hydrostatic load conditions imposed by the requirements.

The study uses mathematical modelling to explore in one and two dimensions the effects of dynamic impact conditions. These conditions are represented by a triangular deceleration pulse and this is imposed on tanks of generalised and wing planform geometry. The study covers response characteristics of one-dimensional tanks for a range of deceleration pulse durations, this provides a predictable dynamic pressure determinant which is then replicated with an analytical solution. Rigid two-dimensional tanks of various configuration are studied, these are used to explore the effects of baffles, sweep angle and pulse duration. Finally flexibility effects are incorporated, both for simple and wing planform tanks. Both overall wing bending and local structural flexibility are modelled.

The study shows that shape effects, elastic deformation and baffling can, in unfavourable circumstances result in increased pressures by comparison with that which would be predicted by hydrostatic analysis. Plastic deformation can result in significant alleviations, the actual level of alleviation is highly dependent on the characteristics of the tank under consideration. Some suggestions are made regarding the substantiation of fuel tanks using dynamic analysis and a need for further study into real emergency landing deceleration characteristics is identified.

Contents

List of Figures

1 INTRODUCTION

This study of the dynamics of rapidly decelerating fuel tanks was initiated by the United Kingdom CAA with the objective of identifying the conservatism or otherwise of the existing fuel tank emergency landing requirements based upon hydrostatic pressure criteria.

The current requirements are presented in JAR 25.963 (d) and (e) which state:

> *25.963 (d) Fuel tanks must, so far as it is practicable, be designed, located and installed so that no fuel is released in or near the fuselage or near the engines in quantities sufficient to start a serious fire in otherwise survivable crash conditions. (See also [ACJ 25.963(d).)]*
>
> *(e) Fuel tanks within the fuselage contour must be able to resist rupture, and to retain fuel, under the inertia forces prescribed for the emergency landing conditions in JAR 25.561. In addition, these tanks must be in a protected position so that exposure of the tanks to scraping action with the ground is unlikely.*

Also, ACJ 25.963(d)

Fuel Tanks: general (Acceptable Means of Compliance)

> *Fuel tank installations should be such that the tanks will not be ruptured by the aeroplane sliding with its landing gear retracted, nor by a landing gear, nor an engine mounting tearing away.*
>
> *Fuel tanks inboard of the landing gear or inboard of or adjacent to the most outboard engine, should have the [strength to withstand fuel inertia loads appropriate to the accelerations specified in JAR 25.561(b)(3) considering the maximum likely volume of fuel in the tank(s). For the purposes of this substantiation it will not be necessary to consider a fuel volume beyond 85% of the maximum permissible volume in each tank. For calculation of inertia pressures a typical density of the appropriate fuel may be used.]*

The emergency landing conditions of JAR 25.561 present ultimate inertia cases which are:

Upward	3.0 g
Forward	9.0 g
Sideward	3.0 g
Downward	6.0 g
Rearward	1.5 g

A strict interpretation of the rule requires the full static head of each tank to be considered, i.e. in the case of the 9.0g forward acceleration this will approach the full longitudinal tip to root length of the wing and can thus result in very high design loads.

Evidence from service experience indicates that transient accelerations considerably in excess of those defined by the requirement may have been sustained without fuel tank rupture, although this is not strictly representative of the requirement case

since in the majority of impacts the tanks have contained much less than the specified 85% of the maximum permissible fuel volume. It has been suggested in the recent past that a rapid dynamic pulse may be less damaging than a hydrostatically applied load since the full pressure load may not have time to develop during the pulse. When reacted by typical fuel tank structures with an elastic/plastic response to load this may also have an ameliorating effect. This led to a suggestion that the use of a pressure head based on local chord rather than the full front to rear tank dimension could be appropriate.

The study described here attempts to quantify the comparative effects of hydrostatic and dynamic loading.

2 INITIAL STUDIES

The deceleration pulse used in this work and throughout the study is based on that required by JAR 25.562 for the dynamic evaluation of seat structures. This pulse is defined by a linear rise in deceleration to a peak followed by a linear fall to zero over a similar interval.

Early work concentrated on identifying fundamental dynamic effects. This was achieved by solution of the one-dimensional wave equation.

$$\frac{\partial^2 u}{\partial t^2} = c \frac{\partial^2 u}{\partial x^2}$$

In the case of an infinitely long one-dimensional tank this approach can be reduced to a simple expression of strain in the fluid at the impact face:

$$\text{Fluid strain at impact face} = \frac{\text{velocity of impact face}}{\text{velocity of sound in fluid}}$$

$$= \frac{\frac{1}{2}\frac{da}{dt}t^2}{c}$$

Where:

$\frac{da}{dt}$ = acceleration gradient of pulse.

t = time elapsed from start of acceleration.

c = speed of sound in fluid.

Therefore, Pressure change due to strain = $\frac{1}{2}\frac{K}{c}\frac{da}{dt} . t^2$

Where: K = Elastic modulus of the fuel in the direction of the deceleration.

= Adiabatic bulk modulus.

If, for a symmetrical triangular pulse:

A = Peak deceleration.

R = Rise time. (time to acceleration peak)

then, for $0<t<R$:

$$P = \frac{1}{2}\frac{K}{c}\frac{A}{R}t^2$$

For $R<t<2R$:

$$P = \frac{1}{2}\frac{K}{c}\frac{A}{R}\left\{t^2 - 2(t-R)^2\right\}$$

For $2R<t$:

$$P = \frac{1}{2}\frac{K}{c}\frac{A}{R}\left\{t^2 - 2(t-R)^2 + (t-2R)^2\right\}$$

The results of this calculation are shown in figure 1. It may be observed from this that a constant pressure exists at the face after the completion of the pulse and that this will be proportional to the nett change in velocity due to the pulse.

To evaluate the dynamics of a finite length one-dimensional tank, a finite difference solution of the wave equation was developed. This was applied to a non-dimensionalised range of finite length tanks allowing the development of a dynamic peak pressure determinant. The notation for this exercise is:

$\frac{ct}{l} \rightarrow$ Non-dimensional tank length parameter,

Where: c = sonic speed in fuel

t = dynamic pulse rise time

l = tank length

$\frac{P_d}{P_s} \rightarrow$ Non-dimensional dynamic pressure,

Where: P_d = peak dynamic pressure

P_s = static head pressure generated by the peak deceleration considered as a static inertia condition

The determinant is shown in fig. 2 for a range of ct/l from 0 to 30. This shows significant overpressures resulting from dynamic effects and clearly indicates tuning effects for certain pulse/tank length combinations.

3 AUTODYN, SOWERBY RESEARCH CENTRE (SRC)

The preliminary studies demonstrated significant differences between static and dynamic conditions which required further study. Any further study would also be required to consider the incorporation of parametric tank shape and flexibility effects.

A research contract was placed with the British Aerospace Sowerby Research Centre to develop the study with the objective of gaining an understanding of the dynamics of the fluid/structure interaction.

This study was broken down into two phases, phase 1 consisted of consideration of the one-dimensional case for comparison with the CAA generated finite difference solution, also, to allow detailed examination of the pressure/time history responses at selected locations within the tank. Phase 2 involved a study into the effects of tank shape using two-dimensional planform tanks. An option of extension into three-dimensions was available if required. The analytical tool for this programme was the Autodyn-2D package from Century Dynamics Inc. This is a finite difference hydrocode developed for the analysis of rapid dynamic events such as explosions and impacts, etc.

3.1 One-dimensional study

Parameters explored were:

Tank lengths of 5 ft, 75 ft and 150 ft
Deceleration peaks of 5g, 15g and 25g
Pulse rise times of 50, 75, 100, 200 and 400 msec.

The analysis options available in the Autodyn code and explored in this study were:

(i) Mesh type

Two types of computational mesh are available, Lagrangian and Eulerian:

Euler meshes retain their original geometry and material flows freely across cell boundaries. Partially empty cells can introduce numerical noise into the solution since they are detected as either full or empty and the transition occurs over a single time step.

Lagrangian meshes distort with the material, i.e. the mass of each cell is constant and there is no flow of material through the cell boundaries. Lagrangian meshes were found most appropriate to this study.

For both mesh types cell properties are based at the centre of the cell.

(ii) Equation of state

Two options were employed, a linear equation of state (LEOS) and a shock equation of state (SEOS)

The linear equation of state defines material response with the adiabatic bulk modulus and a reference density defined at the initial pressure, Sonic

velocity is assumed to be independent of particle velocity. These conditions are identical to those used in the one-dimensional wave equation solutions developed in the early stages of the study.

The shock equation of state modifies the sonic velocity as a fraction of the particle velocity. This approach is most appropriate to very rapid events such as projectile impacts and explosions. For slower events solutions using the SEOS tend towards those of the LEOS. For most solid materials and many liquids, the relationship between shock and particle velocity is linear, but for materials where this is not the case the Mie-Gruniesen equation of state is employed. This relates the pressure within the material to the change in internal energy as a linear function. The two versions of the shock equation of state are:

$U_s = c_0 + S.U_p$

Where: U_s= shock velocity

U_p= particle velocity

c_0 = velocity of sound as defined by the bulk modulus,

i.e. $c_0 = \sqrt{\frac{K}{r_0}}$

S = gradient of Hugoniot characteristic:

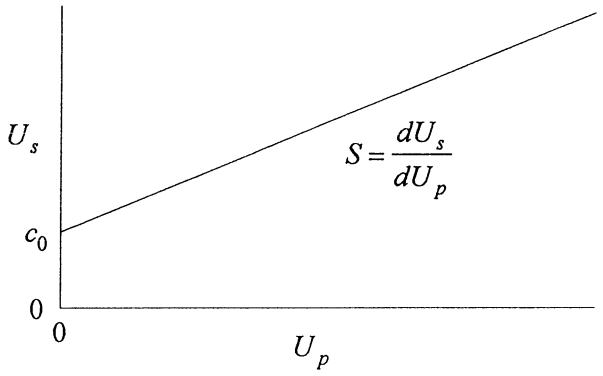

Mie-Gruniesen equation:

$P = P_H + \Gamma\rho_{ref}(e - e_H)$

Where: P_H , ρ_{ref} and e_H are the reference pressure, density and specific internal energy for the Hugoniot characteristic.
Γ = ratio of specific heats, c_p/c_v
e = specific internal energy

(iii) Material characteristics

Shock equation of state: (Paraffin, Ref: Autodyn materials database.)
c_0 = 2960 m/sec. S = 1.531 Γ = 1.18 ρ_{ref} = 900 kg/m^3

Linear equation of state: (Jet A1, Ref: 'Aviation Fuel Properties', Co-ordinating Research council, Society of Automotive Engineers, 1983.)
K = 1110 x 10^6 N/m^2 ρ_{ref} = 786 kg/m^3

A further parameter was the hydrodynamic tensile limit. This is used to simulate the effects of cavitation. Cavitation occurs where the pressure in a liquid falls below the vapour pressure and bubbles of vapour are formed, when the pressure returns these can collapse violently causing short duration spikes of very high pressure. Simulation of cavitation is achieved by giving tensile pressures a limiting value. If pressure falls below this limit the cell pressure is then fixed at this value. Material that has failed in this manner can still support compressive loads and so, if the tensile limit is set to zero, the failed material will continue to behave in a similar manner to the unfailed material during further compressive loading.

A sample of the output from the one-dimensional modelling is shown graphically in figures 3 and 4. These two plots show general agreement of the Sowerby results with the CAA finite difference solution although the low acceleration points appear to overestimate the pressures. This over-estimation arises as a result of simply identifying the highest numerical value in a given pressure/time history, hence the values shown represent the basic pressure pulse plus any numerical or cavitation induced noise that may be present. In the case of the lower acceleration values the noise component is significant.

The effects of cavitation are shown in figure 5. This shows much higher pressures for the 5g case and all peaks are increased slightly. The results of this however are unreliable due to the use of the shock equation of state, which, at the low pressures involved generated very high numerical noise levels. A comparison between the cavitation and no-cavitation pressure time history for a 5ft tank using the linear equation of state is shown in figure 6. This shows a trivial difference to the peak pressure, the major and obvious difference being the residual dynamic oscillation in fuel pressure at the end of the pulse for the no cavitation case. This is due to the non-cavitating fluids ability to support negative pressures and so no mechanism for the dissipation of strain energy is present. Following the primary response, the cavitation response shows a pressure of zero until the travelling wave from the back of the tank reaches the face at about 17msec, the resulting spike is however of low magnitude. This plot was generated from a twenty cell model and this is the cause of the numerical noise evident in the primary pressure rise. As will be seen later, the noise level is sharply reduced at higher mesh densities.

3.2 **Two-dimensional study**

The purpose of this part of the study was to investigate the response of rigid wall two-dimensional planform tanks over a range of pulse lengths and amplitudes similar to that already explored in the one-dimensional work. The effect of partially filled tanks was also to be investigated.

The tank planform selected was based on the Boeing 747–400. This resulted in a straight tapered, swept outer portion with a rectangular unswept centre-section. All

walls were constrained to a boundary condition which enforced motion following the deceleration pulse and hence the walls were constrained and therefore rigid.

Figure 7 illustrates the tank planform used for this phase and Figure 8, a sample of the peak pressures recorded over-plotted on the one-dimensional determinant. This shows a similar characteristic to the 1D results but with an apparent bias to higher ct/l values. The reference length used in data reduction to non-dimensional form was the maximum longitudinal tank length. The dynamic component of the pressure response however is nearly at the fundamental frequency of the tank found by taking the greatest linear dimension, this is similar to a primary result of the one-dimensional work and is shown in Figure 9. The determinant has been scaled along the ct/l axis by the ratio of the greatest tank dimension to the longitudinal tank length to allow a better comparison with the 1D response. Peak overpressures are lower than in the 1D case and this may be explained by diffusion of the reflected pressure waves by the varying angles of the tank wall, this also opens the possibility of pressure amplification due to shape effects. Note also that since the pressure wave reflections in this model are fully elastic, any observed pressure reduction may not be relied upon for other configurations.

SRC also studied the effects of removal of the tank centre section and of part filling the tank. This latter however was achieved by replacing the tank tip with a new hard boundary and so predictably, the results from this phase mimic those from the full 2D tank.

Cavitation effects, where simulated, result in a high amplitude spike after the passage of the main pulse arising as a result of the cavitation closing against the rigid tank boundary. This is similar to the water hammer effect observed in long pipes after the rapid closure of a valve and this accounts for much of the noise present in pressure/time histories seen later in the study.

4 ANALYTICAL MODELLING OF THE RESPONSE OF ONE-DIMENSIONAL TANKS

Prior to CAA acquisition of the Autodyn software and the continuation of the dynamic modelling in-house, an attempt was made to gain a greater understanding of fuel tank dynamics by further analysis of the Sowerby results. It is clearly observed that greater pulse rise times (higher ct/l values) produced responses in which the tank face pressure closely shadowed the static pressure that would be produced by the instantaneous acceleration level. This was expected as the acceleration at any point on an infinite acceleration rise will be constant and the problem reduces to the evaluation of the static pressure head. A regular oscillation about a mean pressure rise gradient was observed. For the shorter pulse lengths this dominates the form of the response and tunes to produce the maximum pressure at ct/l = 2. Examination of time histories for different points along a one dimensional tank and tank longitudinal pressure distributions reveal the oscillatory pulse to be a standing wave with a period of 4l/c. This is the fundamental frequency of the tank (organ pipe frequency). To confirm this observation the observed periodic times where compared with calculated values for a range of the Sowerby results and the errors evaluated, these are tabulated below:

Rise Time (msec)	Peak Acceleration (g)	Period (sec)	Error (%)	Equation of State
50	15	0.0621	0.44	Shock
75	15	0.0614	–0.68	Shock
100	15	0.0610	–1.24	Shock
200	15	0.0604	–2.24	Shock
400	15	0.0624	0.99	Shock
200	5	0.0600	–2.91	Shock
200	25	0.0613	–0.85	Shock
75	15	0.1550	0.74	Linear
100	15	0.1572	2.17	Linear
200	15	0.1531	–0.52	Linear
400	15	0.1541	0.15	Linear
200	5	0.1532	–0.46	Linear
200	25	0.1548	0.57	Linear

The errors found in the above table are within the limits expected from a graphical interpretation.

Once the initial wave front has progressed to the back of the tank the successive rise in deceleration at every point in the tank is linear since pressure signals travel from the impact face at a constant rate. The result of this is that the wave form due to a change in da/dt is fully established at the instant the response induced by this value of da/dt reaches the free face at the back of the tank and is unchanged unless there is a change in da/dt. The elements for an analytical model are therefore a dynamic wave whose form is defined by da/dt and an instantaneous hydrostatic pressure.

For a linear acceleration change:

$$P = \frac{1}{2}\frac{K}{c}\frac{da}{dt}.t^2$$

Where: t = time from initiation of da/dt

As the pressure signal progresses at sonic velocity, this expression can be applied to any point in the tank behind the initial pressure signal, i.e.:

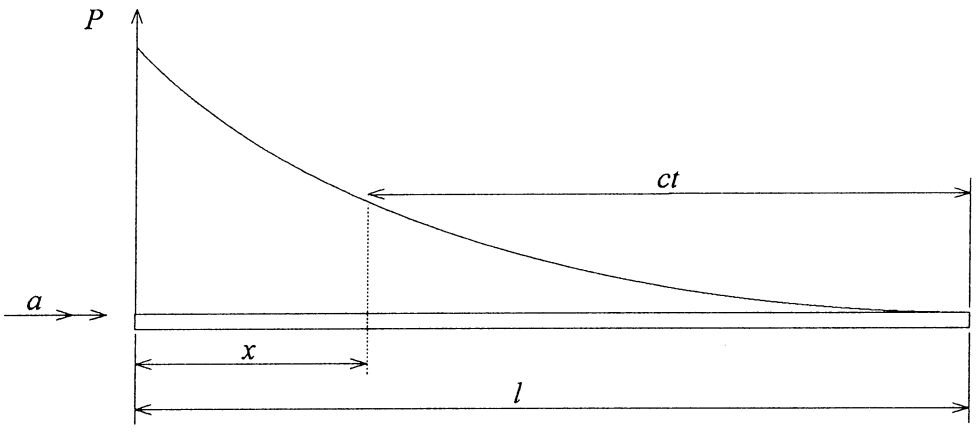

t = Time elapsed at point x since the passage of the initial pressure signal covered by da/dt.

$$t = \frac{(l - x)}{c}$$

And for the initial pulse rise;

$$\frac{da}{dt} = \frac{A}{R}$$

And hence;

$$P_x = \frac{1}{2}\frac{K}{c^3}\frac{A}{R}(l - x)^2 \text{ ———————— (1)}$$

The instantaneous hydrostatic pressure at this point is:

$$P_{s_x} = \rho\, a\, (l - x)$$

$$\rho = \frac{K}{c^2}$$

$$a = \frac{A}{R} \cdot \frac{l}{c}$$

$$P_{s_x} = \frac{K}{c^3} \cdot \frac{A}{R}(l - x)\, l \text{ ———————— (2)}$$

Subtracting (2) from (1) gives the oscillatory pressure component at x

$$P_0 = \frac{1}{2}\frac{K}{c^3}\frac{A}{R}\left(x^2 - l^2\right)$$

Re-writing this expression in terms of t;

$$\text{at point x, } \quad t = \frac{(l - x)}{c} \quad (\text{for } 0 < t < {}^{2l}/_{c})$$

$$\text{so} \quad x = l - ct$$

And hence,

$$P_0 = \frac{K}{c^2}\frac{A}{R}\left(\frac{ct^2}{2} - lt\right)$$

If this expression is evaluated for a range of t from zero to 2l/c the fundamental parabolic half wave for the tank is generated. This may be extended using an odd Fourier series of period 4l/c. i.e.;

$$P = \frac{16KAl^2}{R(\pi c)^3}\left\{-\frac{1}{1^3}\sin\frac{\pi c}{2l}.t - \frac{1}{3^3}\sin\frac{3\pi c}{2l}.t - \frac{1}{5^3}\sin\frac{5\pi c}{2l} \cdot t....\right\}$$

It should be noted that this represents the oscillatory component generated at time t by a constant rate of acceleration change da/dt. If this is to be applied to a long tank then the separate stages of the triangular pulse must be applied cumulatively.

Dissecting the pulse;

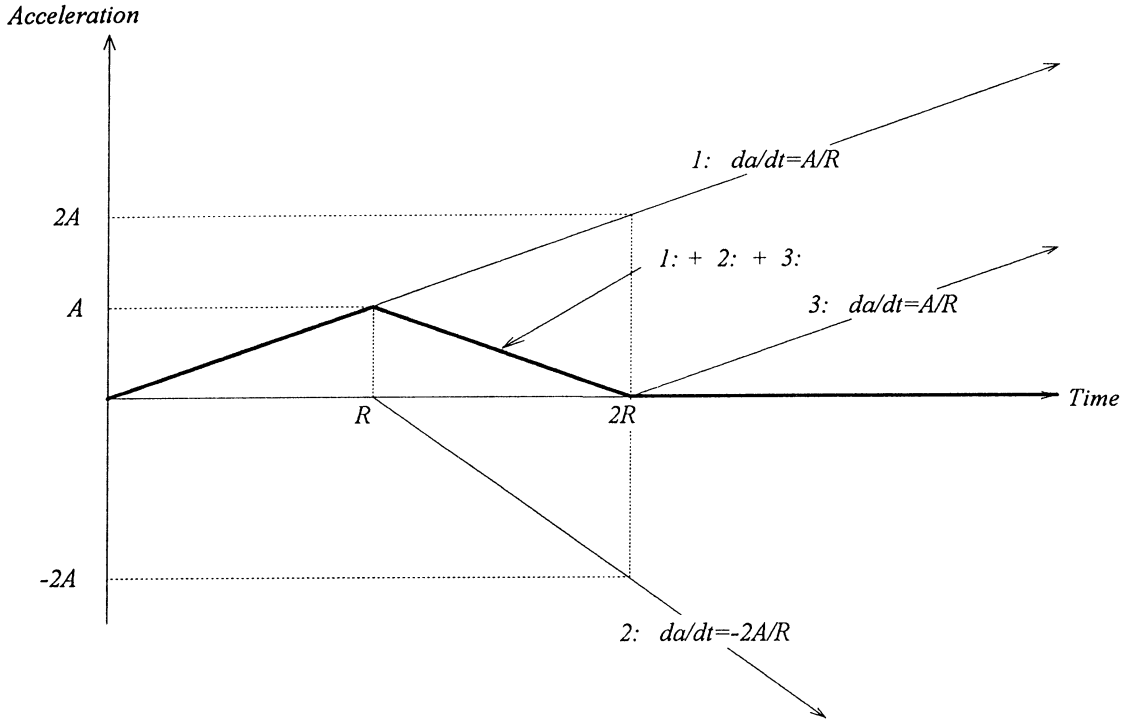

For a constant da/dt, the static component is given by;

$$P_s = \rho a l$$

$$= \frac{K}{c^2} \cdot \frac{A}{R} \cdot t.l$$

So the full pressure/time relationship for a constant da/dt is;

$$P = \frac{KA}{R}\left\{\frac{tl}{c^2} + \frac{16l^2}{(\pi c)^3}\left[-\sin\frac{\pi ct}{2l} - \frac{1}{3^3}\cdot\frac{\sin 3\pi ct}{2l} - \frac{1}{5^3}\cdot\sin\frac{5\pi ct}{2l} \ldots\ldots\right]\right\}$$

This expression may be used directly for $0<t<R$, appropriate expressions representing the conditions of phases 2 and 3 of the pulse must be added at $t = R$ and $t = 2R$ to generate the full response. Pressure histories have been evaluated for a range of ct/l from 1 to 4 using this approach and are illustrated in figure 10. This figure shows the effect of tuning at ct/l = 2 as may be observed from the determinant (Fig. 2). Tuning is dependant on the maximum possible pressure rise gradient occurring at $t = R$ (to give the greatest possible overshoot). This occurs if the number of full oscillatory cycles prior to the acceleration peak is $n + (1/2)$ where n is an integer greater than or equal to zero, and ct/l is thus the number of half cycles prior to the acceleration peak. Evaluation of the determinant using this approach also reveals the P_d/P_s = 1 at 1, 4, 5, 8, 9, 12, 13 ….. etc, the determinant shown in figure 2 was developed using the earlier finite difference program and some numerical error is evident in the frequency of the curve. The determinant for 0 < ct/l < 5 from the analytical model is shown below for comparison:

**Determinant with non-dimensional tank length parameter.
Analytical model.**

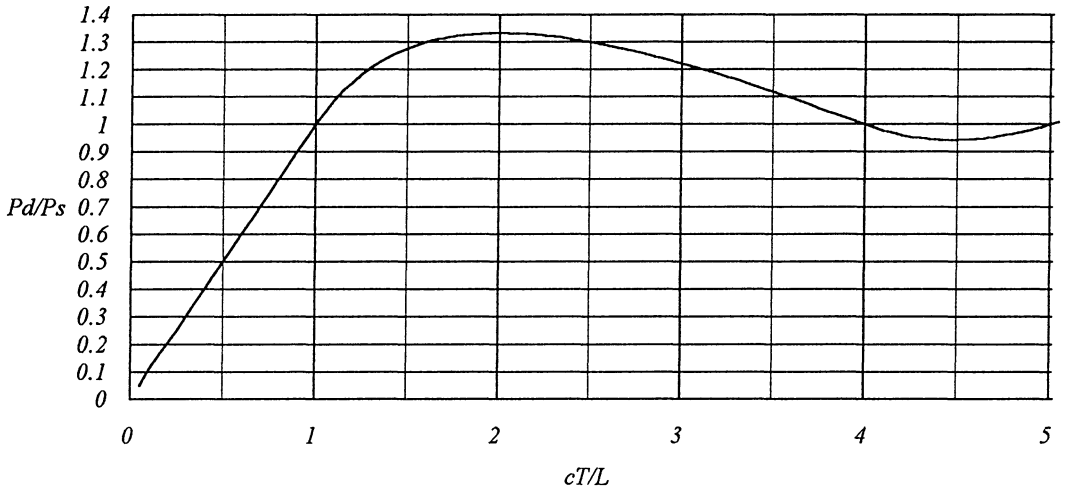

Figure 11 presents a pressure/time comparison between a non-cavitating Autodyn model and the analytical model.

5 AUTODYN, CAA

With the acquisition of the Autodyn package by the CAA Structures Department, the research was continued as an in-house project. The stages of the project consisted of verification of the Autodyn software by comparison of one-dimensional models with the wave equation solution, exploration of the effects of shape on rigid walled two-dimensional tanks, the effects of rigid baffles, development of flexible wall models with crushing properties similar to aircraft structure, effects of fore and aft wing bending stiffness and finally a flexible wall model with flexible baffles incorporating fore and aft bending.

5.1 Rigid one-dimensional tanks

This phase was used to gain familiarity with the Autodyn software and to establish confidence in the results. To this end, a family of 10 tanks were evaluated for a range of ct/l from 1 to 13 and to provide a quasi-static solution at ct/l = 118. The results of this exercise are shown in figs 12 and 13 in comparison with the output from the 25 point finite difference model. All Autodyn P_d/P_s values are lower than the correct analytical value due to the output data being referenced to the cell centre, this gives an associated reduction in static head. This is also the case at ct/l = 118 where the result is dominated by the static head. Reference to figure 11 reveals the close agreement with the analytical model (with no cavitation hence the remaining oscillation at t > 100 msec).

Special deceleration boundary conditions were defined on CAA's behalf by Century Dynamics allowing the easy imposition of a triangular pulse of any duration and peak deceleration value.

5.2 **Rigid two-dimensional tanks**

5.2.1 *Simple rectangular tanks*

Before wing planform tanks were attempted some simple geometric forms were tried. The first of these was a rectangular tank 12.5 m x 5.0 m. This was exposed to two pulses, the first at *ct/l* = 4 where *l* was the tank width. The tank was rotated in 22.5° steps from a starting point with *l* = 12.5 m until the tanks major axis was normal to the acceleration vector. At each rotational position the model was allowed to run until the pressure at the face returned to zero. The pressure – time histories for these runs are shown in Figure 14 and a plot of the P_d/P_s ratio vs *ct/l* in Figure 15 (*l* in this case refers to the maximum dimension parallel to the acceleration vector). Although a close agreement with the equivalent one-dimensional result (within the likely error limits of Autodyn) occurs at both the 0° and 90° rotations, the progression through the intermediate rotations indicates that tank boundaries that are not orthogonal or parallel to the acceleration vector have a diffusing effect on the dynamic response, i.e. P_d/P_s tends towards unity for most values of ct/l. Figure 16 includes the results of the second family of runs with a 50msec pulse rise time. This shows a continuation of the trend towards P_d/P_s = 1 although the last point has suffered from an effective truncation of tank head due to the cell centred data reference points, this is further aggravated by the small number of cells over the tanks minor axis. It is however clear that the simplistic one dimensional determinant approach is no longer valid, although it is still quite possible to achieve transient pressures in excess of the static head value, particularly at low ct/l values.

5.2.2 *Skewed rectangular tanks*

As a means of gaining a greater appreciation of the effect of increasing the maximum dimension of a tank (in search of tuning effects) while maintaining the same static head dimension, a model was developed in which an initially rectangular tank was progressively skewed to a parallelogram with the flat front and rear faces remaining the same distance apart in the deceleration direction (see Figure 17). The outputs from this model are shown in Figure 18 in comparison with the determinant. Since, with respect to the deceleration vector, this tank retains its geometric character with increasing skew, a comparison with the determinant is more likely to be valid than for the rotated tank. *ct/l* has been calculated using the maximum (corner to corner) dimension of the tank whereas the equivalent maximum static pressure uses the fixed deceleration vector direction length (12.5 m in this case). Although the dynamic pressures generated are lower than those for a 1D tank it is evident that possibilities for tuning, with the attendant risk of developing significant overpressures, still exist for tanks of more complex geometry. Figures 10 and 19 illustrate the similarity of this models response to the one-dimensional tank. Figure 10 shows the analytical time histories at the pressure face for a range of 1D tanks of increasing ct/l. Figure 19 shows the pressure face time histories for the increasingly skewed tank. Although the skew tank results are more irregular, it is clear that the shortest of these tanks (rectangular) is identical to a 1D response with nearly 5 quarter cycles of the oscillatory component occurring within the rise time, the actual ct/l value being 4.754. The fully skewed tank, (skew 5) has a ct/l of 2.126, and as predicted from the earlier 1D work is nearly tuned for maximum overpressure (2 quarter cycles to the pulse rise time).

5.2.3 *Exploration of baffle effects*

The initial study of baffle effects utilised the same rigid rectangular tank described in section 5.2.1, but in this case, with a dividing transverse porous baffle across the centre (see fig 17). The baffle is defined by its porosity, i.e. a 40% baffle closes off 40% of the overall tank cross sectional area. Since the Autodyn models are constructed from a group of discrete cells it was not possible to achieve fine detail within the baffle without making the model excessively large and thus increasing computing times to an unacceptable level (some runs for the baffled tanks took in excess of three hours), as a way round this problem, all peak pressure data from the simple rectangular tank is achieved by taking an average across the pressure face and the baffle was represented as a solid barrier partially blocking the tank. This was considered reasonable since for the deceleration vector shown in Figure 17 the longitudinal edges of the tank are effectively reflection planes and so the tank has infinite width, as a result of this, the baffle is in effect finely segmented when compared with the (infinite) width of the tank.

Although rigid baffles were not expected to be an efficient method of dissipating strain energy within the fuel, a primary objective of this particular model was to identify the effect of the baffle on the dynamic wave form. Figure 20 shows the typical effect of a 75% baffle on this tank, it is of interest to note that (ignoring the small oscillations) the overall dynamic oscillation has increased in wavelength, i.e. the effective dynamic tank length has increased. Although the underlying quasi-static response is little changed, the change in wavelength has altered the tuning with the result that the peak pressure is actually slightly higher than that for the un-baffled tank. Examination of the detailed pressure wave motion within the tank shows that the two half tanks either side of the baffle have their own independent cyclic pressure waves. The pressure response at the tank face is then a result of the constructive/destructive addition of these wave systems. If the response for a range of ct/l values is evaluated, given the above observation, the resulting determinant should indicate that the tank is dynamically larger than its geometric length, i.e. the determinant should shift to the right. This has been evaluated for two baffle fractions (50% and 75%) and presented as Figure 21, the expected shift is evident.

Although the altered tuning can in itself increase the dynamic pressure, figure 21 also shows that the amplitude of the determinant has increased, particularly at low ct/l values and hence it is of interest to explore the variation of peak pressure with baffle fraction at a constant ct/l value. Figure 22 shows the effect of varying the baffle fraction from 0 to 1 at $ct/l = 1$, for which a 1 dimensional tank produces the same peak pressure both statically and dynamically. Although not conclusive due to the single ct/l value, this does show that a rigid baffle has no appreciable benefit until it forms an almost impermeable barrier across the tank.

The most significant conclusion that may be drawn from the foregoing is that rigid tanks do not have an effective mechanism for diffusing elastic pressure waves and hence, by design or misfortune, may generate dynamic pressures significantly in excess of those generated hydrostatically.

5.3 **Flexible tanks**

5.3.1 *Definition of boundary conditions*

Due to the limitations of the Autodyn software, the modelling of structural flexibility required adaptation of an existing material model rather than an attempt to model real structure. The constraints on this process were:

(a) A two-dimensional simulation of a three-dimensional effect.

(b) The need to keep the time taken for a sonic wave to cross each cell as large as possible. This is because the computational time steps are defined by the shortest time to cross any cell and so a very small cell, or a high sonic speed for the cell material, will lead to unacceptably long computation times.

(c) Any boundary material model needed a clearly defined failure. Cell by cell interpretation of material state is too cumbersome for efficient computing.

Of the various material models available within the Autodyn package, the 'porous' equation of state appeared most appropriate. This model was originally intended for the simulation of concrete and structural foams. It allows for an initial elastic compaction of defined gradient followed by a piecewise linear plastic phase with elastic recovery at the original stiffness, to a fully compacted form which is fully elastic, again at the original elastic stiffness. This is illustrated graphically below:

Expansion and recompaction is computed from:

$$\frac{\partial P}{\partial \rho} = c^2$$

Where c=solid sound speed.

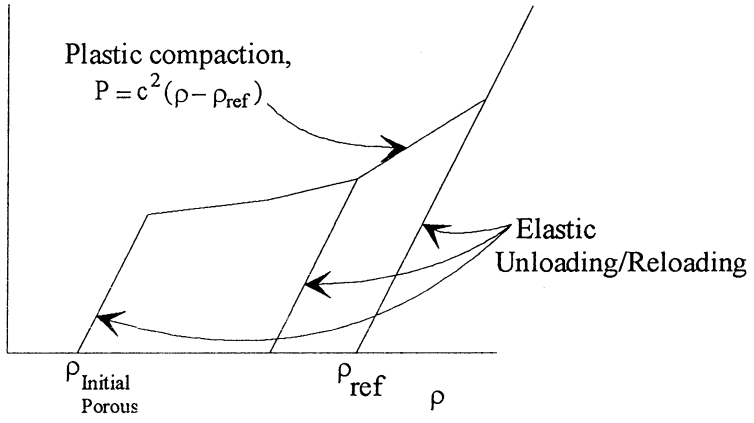

The flexibility of a real tank is complex with many interactions between the upper and lower skins, baffles, webs, stiffeners and other structure. Since the purpose of the study was to identify generic effects rather than to attempt detailed modelling of real structure, it was decided to reduce the problem to defining a boundary stiffness of the correct order of magnitude to provide a fair indication of the likely effects of real structure/fluid interactions. As all the modelling for this study was either one or two dimensional, any attempt to generate accurate and generally applicable quantitative results for a real three-dimensional tank would have been of questionable value and unnecessary for the purposes of a parametric study.

An idealised tank boundary structure was defined to allow the constants for the porous material model to be defined. This comprised a flat plate spar web stabilised with L section stiffeners and is illustrated below:

Simulation of web structure for input to the Autodyn porous material model

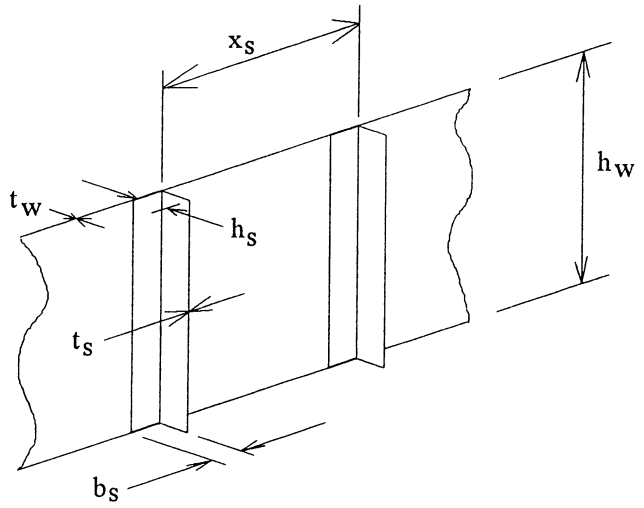

Material: 3L72

Stiffener spacing:	x_s	=	20 cm
Web height:	h_w	=	30 cm
Stiffener foot width:	b_s	=	3 cm
Stiffener flange height	h_s	=	4 cm
Web thickness:	t_w	=	0.4 cm
Stiffener thickness:	t_s	=	0.4 cm
Youngs modulus:	E	=	72000MN/m^2
Material density:	ρ	=	2.79gm/cm^3
Porous sonic reference velocity:	c	=	38.896cm/msec
Tensile yield stress:	σ_y	=	260MN/m^2
Tensile failure stress:	σ_f	=	3930MN/m^2
Tensile failure strain:	ε_f	=	0.13

To convert the response of this structure into material properties it was first necessary to define the deformation characteristics, these then allowed the evaluation of the material volumetric response to pressure loading. Simplifying assumptions made for this process were:

1 Each panel (bounded by two stiffeners) was assumed to be equivalent to a flat plate with two edges (top and bottom) simply supported and the remaining two edges fixed.

2 To simplify the calculation of the volume swept out by the deflecting panel, the deflection form was assumed to be approximately sinusoidal. This simplification was considered to be acceptable in the context of the other approximations implicit in two-dimensional modelling of complex three-dimensional problems.

3 Elastic deformation of the structure was assumed to be linear with pressure.

4 Plastic deformation was assumed linear to the failure point which was defined by the achievement of tensile failure stress in the stiffener.

5 Elastic stiffness was assumed to be unchanged by previous plastic deformation.

For the structure defined, the elastic neutral axis is located at:

$$y_{NA} = \frac{\frac{x_s t^2{}_w}{2} + b_s t_s t_w + \frac{b_s t^2{}_s}{2} + \left(t_s h_s - t_s^2\right)\left(t_w + t_s + \frac{[h_s - t_s]}{2}\right)}{x_s t_w + t_s b_s + t_s (h_s - t_s)}$$

where y_{NA} is the distance of the neutral axis from the web face. The section second moment of area is given by:

$$I_{yy} = \frac{1}{3}\left\{x_s y^3{}_{NA} + x_s\left(t_w + h_s - y_{NA}\right)^3 - \left(x_s - t_s\right)\left(h_s + t_w - y_{NA}\right)^3 - \left(x_s - t_s - b_s\right)\left(y_{NA} - t_w\right)^3 + \left(b_s - t_s\right)\left(y_{NA} - t_s - t_w\right)^3\right\}$$

The elastic volumetric stiffness may be considered as comprising of two components, i.e. pressurisation of the web with the edge constraints as defined in assumption 1 above, and deflection of the whole web assembly by bending deformation of the stiffeners between the upper and lower skins. The two effects are assumed to be approximately independent and hence linear superposition may be applied.

For the web plate, Roark 'Formulas for stress and strain' gives the following expression for the maximum elastic deformation of a plate constrained as defined;

$$y_{max} = \frac{-\alpha q x_s^4}{E t_w^3} \quad \text{---------- (5.3.1)}$$

Where: α is a tabulated coefficient for a range of values of h_w / x_s, i.e.;

h_w / x_s	1	1.2	1.4	1.6	1.8	2
α	0.0210	0.0349	0.0502	0.0658	0.0800	0.0922

q = Applied pressure loading.

Using assumption 2 (harmonic deformation), the deflected form for any horizontal slice is:

$$y_x = \frac{Y}{2}\left\{cos\left(\frac{2\pi x}{x_s}\right) - 1\right\}$$

where:

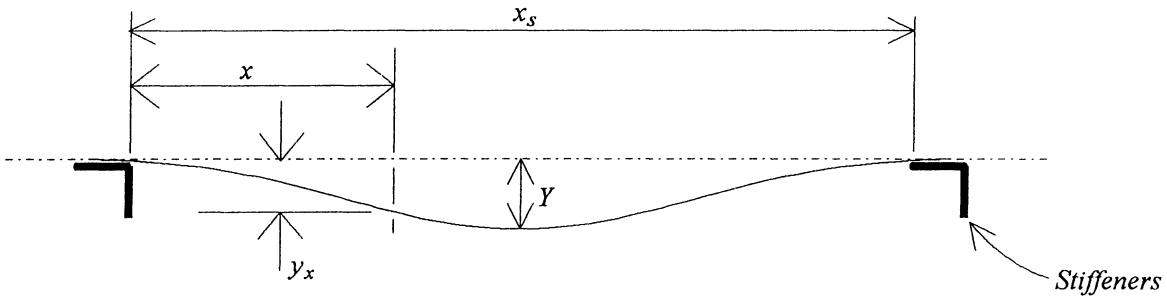

The area swept out by this deflection is:

$$s = \frac{Yx_s}{2}$$

And similarly, for the central panel vertical slice:

$$y_x = y_{max} \sin\left(\frac{\pi x}{h_w}\right)$$

Where

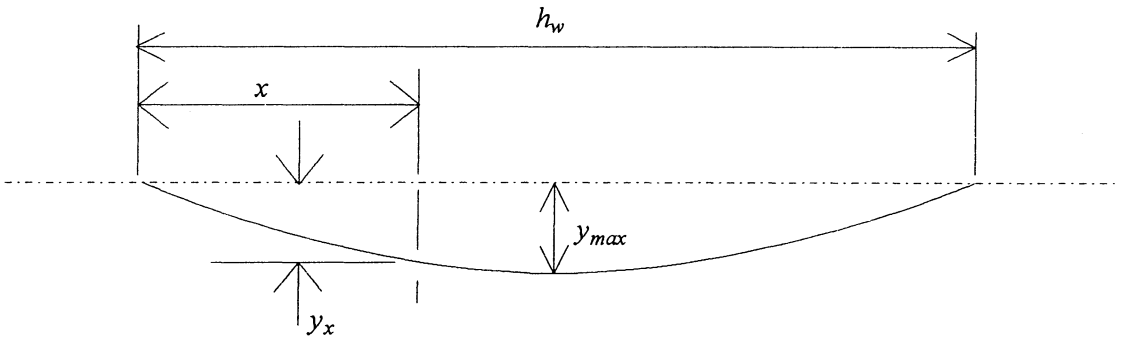

Note: y_{max} in this case is the centre panel deflection.

The area of a slice at x is thus:

$$S_x = \frac{\left\{y_{max} \sin\left(\frac{\pi x}{h_w}\right)\right\} x_s}{2}$$

Integrating this between x = 0 and x = h_w gives the volume swept by the deflecting panel, i.e.;

$$\text{Volume} = \sum_{x=0}^{x=h_w} \frac{y_{max}\, sin\left(\frac{\pi x}{h_w}\right) x_s}{2}.\delta x$$

$$= \frac{y_{max} x_s}{2} \int_0^{h_w} sin\left(\frac{\pi}{h_w} x\right) dx$$

$$= \frac{h_w x_s y_{max}}{\pi} \text{ ---------- (5.3.2)}$$

Considering the web as a beam (for stiffener bending);

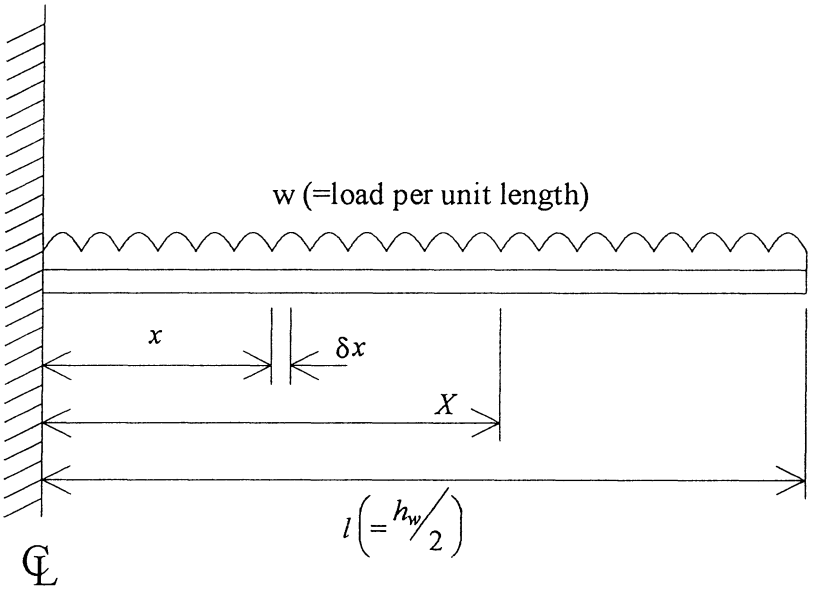

$$M_x = \frac{(l-x)^2 w}{2}$$

Radius of curvature at x;

$$R_x = \frac{EI}{M_x}$$

Hence the change of slope over δx;

$$\delta\theta = \frac{(l-x)^2 w}{2EI}.\delta x$$

And,

$$\theta_x = \int_o^x \frac{(l-x)^2 w}{2EI}.dx$$

$$= \frac{w}{EI}\left[l^2 x + \frac{x^3}{3} - lx^2\right]$$

Deflection;

$$y_x = \int_o^x \theta \, \delta x$$

$$= \frac{w}{2EI}{}_0^x \left[\frac{l^2 x^2}{2} + \frac{x^4}{12} - \frac{l x^3}{3} \right]$$

y_{max} occurs at X=1, so;

$$y_{max} = \frac{w l^4}{8EI}$$

The area swept by the deflected beam, i.e. inside the deflection curve;

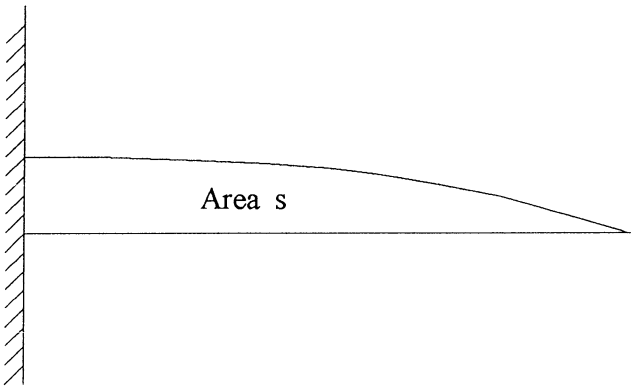

$$s = \frac{3wl^5}{40EI}$$

Note that $l = \frac{h_w}{2}$, so;

$$S = \frac{3wh_w^5}{640EI}$$

w = Pressure x x_s and hence,

$$s = \frac{3Px_s h_w^5}{640EI}$$

giving a displaced volume per bay of;

$$v = sx_s = \frac{3Px_s^2 h_w^5}{640EI}$$

The total volume displaced by elastic deformation is thus:

v = Volume due to web deflection + Volume due to stiffener deflection

$$= \frac{P}{E}\left\{ \frac{3x_s^2 h_w^5}{640I} + \frac{\alpha h_w x_s^5}{\pi t_w^3} \right\} \text{ ---------- (5.3.3)}$$

To provide an approximation to the effects of plasticity some further assumptions were required.

1 The deflected form is unchanged by plastic deformation.

2 The failure criteria is ultimate tensile strain in the stiffener. Following failure the material has no further resistance to pressure loading other than that provided by its own inertia.

3 The neutral axis location is unchanged by plastic deformation. Tensile failure in the stiffener free flange is the only scenario considered since the neutral axis location will cause this area to experience the highest strain.

Although these deflections and failure criteria are a gross simplification of the real situation it must be remembered that the limitations of two-dimensional modelling will only allow 'ball park' reality and hence response of the correct order of magnitude only is sought.

The maximum bending moment occurs at the centre of the stiffener;

$$M_{max} = \frac{P x_s h_w^2}{8}$$

The plastically deformed beam is assumed to carry the following stress and strain distributions just prior to failure:

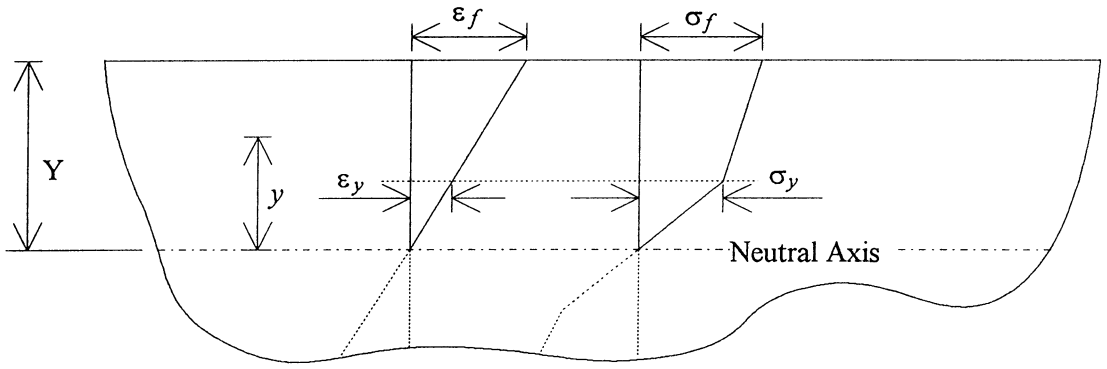

$$\varepsilon_y = \frac{\varepsilon_f}{Y}.y$$

Where y = distance from neutral axis

$$y_y = \frac{\varepsilon_y}{\varepsilon_f}.Y \text{ ---------- (5.3.4)}$$

Note: suffix y refers to the material yield condition.

Since the free limb of the stiffener is of uniform thickness (t_s), the moment resisted by the section under this condition is:

$$M_{max} = 2\int_0^Y t_s.\sigma(y).y\ dy$$

Noting that $\sigma = F:(y)$

For the elastic core of the stiffener;

$$M = \frac{\sigma I}{y}$$

$$= \frac{2\sigma_y\ t y_y^2}{12}$$

And so the overall moment on the section at failure loading is given by:

$$\frac{M_f}{2} = \frac{\sigma_y t_s y_y^2}{12} + t_s \int_{y_y}^{Y} \left\{ \sigma_y + (\sigma_f - \sigma_y) \frac{(y - y_y)}{(Y - y_y)} \right\} y\ dy$$

$$= \frac{\sigma_y t_s y_y^2}{12} + \frac{t_s}{2}\left[\sigma_y - \left(\frac{\sigma_f - \sigma_y}{Y - y_y} \right) y_y \right] (Y^2 - y_y^2) + \frac{t_s}{3}\left[\frac{\sigma_f - \sigma_y}{Y - y_y} \right] (Y^3 - y_y^3) \quad \text{----------(5.3.5)}$$

The yielding moment is:

$$M_y = \frac{\sigma_y I}{Y}$$

Use of the above derivations for the elastic case allows a volume change per unit web area to be defined for the web structure. Equation (5.3.3) gives the deflected volume of one inter-stiffener bay, if this is divided by the bay area ($h_w X_s$) the mean linear deflection of the web will be given. This may be defined for the yield point by setting $y_y = Y$ and so:

$$M = \frac{l^2 w}{2} = \frac{\sigma_y I}{Y}$$

$$= \frac{h_w^2 P x_s}{8}$$

$$\text{Therefore, } P_y = \frac{8\sigma_y I}{h_w^2 x_s Y}$$

Entering this pressure in equation 5.3.3 will give the volume change at yield. The failure moment on the section is given by equation 5.3.5, which, in a similar manner to the yield point moment (above) will give the failure pressure, i.e.:

$$M_f = \frac{h_w^2 P x_s}{8}$$

$$\text{Hence, } P_f = \frac{8M_f}{h_w^2 x_s}$$

The strain associated with this is known (for the free edge of the stiffener) and hence an approximate failure volume change may be found by factoring the yield volume.

$$V_f \approx \frac{\varepsilon_f}{\varepsilon_y}.V_y$$

A density for the material was selected to approximate the mass of the deformed structure at the failure point (since the mass is collected as the material deforms). This in turn gives the material sonic velocity since, from the material model $c^2 = dp/d\rho$. The resulting material characteristic is shown below:

Porous material model for simulation of structural deformation and failure

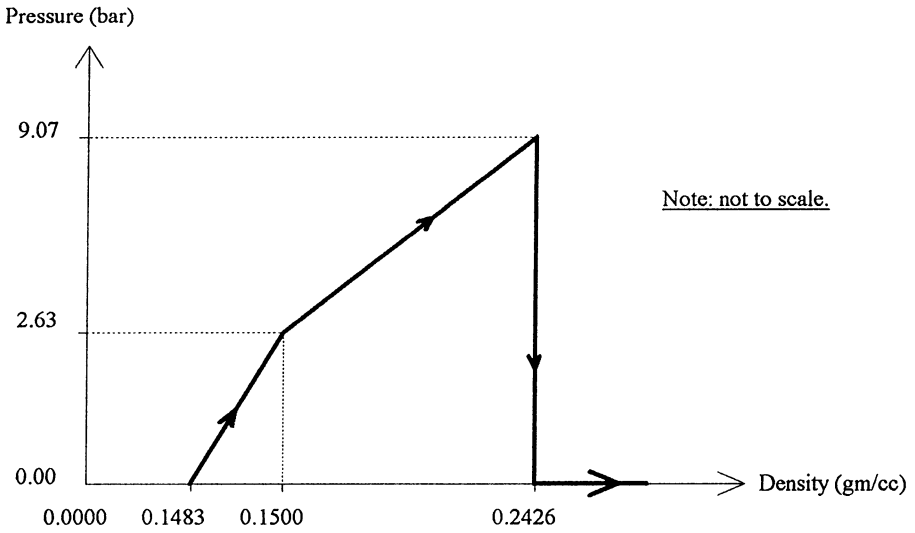

Note that for this application complete compaction has not been used, instead the piecewise linear plastic compaction region has been used to simulate complete failure. This is achieved by defining the compaction path from the failure point as a vertical line to $P = 0$ (pressure returning to zero with no further compaction) and then further compaction occurs without pressure response.

5.3.2 One-dimensional tanks

A one-dimensional model was developed to explore the characteristics of the material defined in the last section. The deceleration peak was set to just achieve failure pressure at the tank leading face under static conditions and the deceleration boundary condition was applied to a single cell pad of the material, the fuel grid was attached to this pad. A time history for this model is shown in figure 23 for a rise time of 30msec. Also included in this figure is a re-run of the model with a higher deceleration to illustrate the failure condition. The simplistic nature of the model is evident in the sharp discontinuity at the yield point and this generates a detectable pressure response which is visible as an echo at about 30msec for the non-failure case and 27msec for the failed tank. For the non-failure case, the recovery to zero pressure occurs rapidly when compared with the pressure rise, this is due to the non-reversible absorption of energy by plastic deformation of the tank. The failure case is similar until the point of failure (which occurs at a pressure marginally in excess of the static failure pressure) when, due to the material definition, pressure

returns to zero instantaneously. The reason for the slight overpressure is unclear, although it may be due to numerical inaccuracies inherent in the finite difference approach employed by Autodyn.

The determinant for a one-dimensional flexible faced tank is shown in Figure 24. This shows a clear reduction in peak pressure by comparison with that from both the rigid walled tank, and the hydrostatic condition up to the point of failure. A clear discontinuity is observable at the failure point although this is artificially rounded by the data point spacing (failure actually occurs between ct/l =3 and 3.5). The previously noted overpressure is evident for the failed condition in that the post failure line occurs at P_d/P_s = 1.026 although the 2.6% error implicit in this is within the error limits previously observed for the Autodyn software. The yield point will also generate a discontinuity but since this occurs at ct/l<0.5 it is of no significance for a practical fuel tank (for a typical wing tank a 90 msec pulse rise time gives $ct/l \approx 12$).

5.3.3 *Two-dimensional tanks*

A simplified wing planform tank was chosen for this phase of the study. The dimensions of this were based on the Boeing 757 but excluded the dry bay, rib locations were selected for convenient modelling rather than true representation. The Autodyn model is shown in figure 25.

Flexibility was introduced to this model in two components. Wing fore and aft bending and local structural flexibility using the porous material model.

The bending flexibility was achieved by generating a sub mesh, the mass and stiffness of this being tuned to give the same fore and aft first mode bending frequency as a real wing (in this case 2Hz). The fuel mesh and sub meshes representing baffles where then superimposed on this substrate and the lateral frequency again checked, this allowed the response to be fine tuned back to 2Hz, this response is illustrated in figure 26.

Although the bending response of the tank is fully elastic and therefore unlikely to diffuse any dynamic effects, the flexibility from this source is sufficient to have a significant effect on the determinant. Evidence from the one-dimensional flexible model indicated that pressure response was slower by comparison with that from a rigid tank and so the effective ct/l value for a given pulse was expected to be reduced. It will also be noted that the skewed tanks modelled in section 5.2.2 exhibited this effect due to the harmonic length of the tank being increased in relation to the longitudinal length (i.e. the pressure wave tends to run along the greatest tank dimension). The response of the tank modelled with only the bending flexibility represented clearly shows this effect (fig 27) with the first half cycle of the determinant extending beyond ct/l = 10 compared with ct/l = 4 for the one-dimensional case. This has potential significance in that a realistic pulse (say 90 msec rise time) is a slow event in terms of the dynamic response of a rigid tank and pressures approximating to the hydrostatic peak may be expected, the delaying effects of flexibility mean that dynamic effects are still evident above ct/l = 10 and so dynamic dissipation of pressure is still worthy of further consideration.

Local flexibility was introduced into the model initially down the leading edge, the fore and aft bending stiffness still being included and the model initially run with a 9g, 90msec rise time pulse. This is shown in figure 28 and a clear reduction in pressure is evident (the 'No baffles' trace). A determinant was produced for this

configuration and this is illustrated in figure 29. Over the range of *ct/l* covered (0.5 to 15) this shows an overall reduction in pressure. This graph was computed for a peak deceleration value of 16g (the JAR 25 seat deceleration pulse peak) and failure of the web structure finally occurred at around *ct/l* = 10. The hydrostatic failure deceleration for this tank is 13.6 g, i.e. a 15% pressure reduction due to dynamic effects.

Seven flexible baffles were introduced into this model (visible in figure 25) using the same porous material model. These were connected to the fuel mesh such that no venting was represented and the baseline 9g, 90msec pulse re-run, this is also shown in figure 28. A substantial pressure reduction results from this although the response was spoilt by cavitation spikes reflected from the rigid rear wall of the tank and the curve as shown has been heavily filtered. It was not practical to model a flexible rear wall as each run of the model was now taking in excess of one hour and any further increase in model complexity would have made the development of a determinant impractical.

The determinant for this tank is presented in figure 29 and appears to be a scaled down version of the one-dimensional response. This however is a dubious conclusion and is not supported by direct observation of the elastic pressure waves within the tank. The points plotted are also subject to interpretation due to the presence of cavitation spikes, beyond *ct/l* = 10 these spikes made further interpretation impossible. The time history for *ct/l* = 15 has been plotted for the wing root and a mid-span location (figure 30) to illustrate this problem. The form of this response is notably different from that shown in figure 28, the major difference being the level of deceleration (16 g) which results in greater yielding of the web and baffles. It is interesting to note that, except for the runs at *ct/l* = 0.5 and 1, the highest pressures anywhere in the tank still occurred at the tank root, both the exceptions occurred outboard of the mid-span baffle. These values of *ct/l* are so low as to be of no significance to a real tank.

The baffles at this stage were un-vented and it has already been shown (section 5.2.3) that even a small leak can entirely negate the effect of the baffle. Four further runs were therefore made with one node at the rear of each baffle disconnected from the fuel mesh. These points are also plotted on figure 29 and although the tank did not fail, the determinant is much closer to that for the unbaffled case although a significant reduction in pressure from the hydrostatic case is still evident.

6 DISCUSSION AND CONCLUSIONS

6.1 Rigid tank effects

The study has shown that dynamic analysis of rigid walled tanks does not give a reliable relief on design pressures over hydrostatic analysis. Although one-dimensional analysis gives a predictable result as evidenced by the determinant (figure 2), extension into two-dimensional tanks with boundaries that are not orthogonal with respect to the deceleration vector tends to result in a reduced amplitude for the determinant and the peak pressure response tends towards that found hydrostatically.

Simple two-dimensional geometries, for example the skew tank shown in figure 17, give a response similar to the one dimensional determinant, but in this case, the

tuning dimension is the greatest linear dimension of the tank and since this is greater than the hydrostatic length, the determinant appears stretched in the direction of the ct/l axis and dynamic effects retain their significance to higher *ct/l* values.

Rigid baffles when added to rigid fuel tanks have been shown to be ineffective unless they are of near to zero porosity. The response shown in figure 22 indicates that the wrong combination of tank and baffle can result in increased dynamic pressures.

6.2 Flexible tanks

The flexible models employed in this work were highly simplified when compared with a real wing tank due to the limitations imposed by computer power and the two-dimensional analysis code. The results should therefore be regarded as generalised observations rather than as strictly quantitative.

Although the representation of local structural deformation used in this study is very simplistic, it does appear that significant alleviations on design pressures may be realised. Fully elastic deformation does not provide a reliable pressure reduction since by definition, no damping mechanism can exist, plastic deformation however, in combination with the shape effects already noted, can result in reduced dynamic pressures for relatively slow dynamic events. The addition of plastically deformable baffles can assist this effect, but as previously noted, any porosity in the baffles significantly degrades their effectiveness.

6.3 General discussion

If dynamic analysis is to become a viable technique for the design of fuel tanks, a realistic emergency landing scenario must be defined, either for direct application to a numerical model of the aircraft, or to develop a realistic deceleration pulse.

An aircraft sliding on a flat surface is very unlikely to generate longitudinal decelerations that will be problematical for a typical fuel tank. However, service experience has shown that runway overruns often result in the aircraft striking an earthwork or similar obstruction.

If a typical obstruction geometry can be identified, say for example, a ramp of a suitable gradient, then a dynamic structural analysis similar to those already performed in the automotive industry could define the deceleration profile at the tank location. It is unlikely that all aircraft will show similar deceleration characteristics under these conditions and so, while a conservative deceleration could perhaps be defined, a better approach would be to establish a requirement obstruction to be used in conjunction with a defined crash landing velocity and then allow a full dynamic structural analysis to be performed as an alleviation from the hydrostatic head requirement.

6.4 Conclusions

The results of this study do not support the view that a static head based on the local chord will be representative of dynamic conditions. The flexible planform tank model incorporating seven impermeable flexible baffles does provide an alleviation compared to an un-baffled tank, but this effect is seriously degraded when the baffles are not fully impermeable.

Dynamic analysis of a real fuel tank exposed to a triangular deceleration pulse of realistic duration (of the order of 90 msec rise time) is likely to result in design pressures significantly below those that would be obtained by hydrostatic analysis using the peak deceleration level from the same pulse. Most of this pressure reduction can be expected to arise as a result of plastic deformation of the structure.

No general rule (e.g. a lower static ultimate inertia loading) can be defined due to the many permutations of structure and tank shape. The duration and peak deceleration of the pulse also requires further consideration and, in the absence of better information, the dynamic seat pulse (16g, 90msec rise time) would provide a viable starting point although figure 29 shows that vented baffles, for the simplified tank, plus bending and leading edge flexibility, would still fail to reduce pressure to that expected from a 9g hydrostatic analysis, this however is likely to be due in part to the many simplifying assumptions.

As an interim position, credit should be given to design organisations prepared to perform an adequate three-dimensional dynamic structural analysis. However, since a suitable dynamic pulse has yet to be defined for a fuel tank consistency with existing requirement dynamic crash scenarios should be maintained. Pending further work on definition of a suitable pulse an acceptable position would be:

Either of the following must be considered:

> *(i) Fuel tanks must withstand the fuel inertia pressures arising as a result of the emergency accelerations as specified in JAR 25.561(b)(3) considering the maximum static head available within the tank in the same direction as the acceleration vector. A fuel volume equal or greater than 85% of the maximum volume of each tank must be considered, or;*
>
> *(ii) A dynamic analysis using a method acceptable to the authority must be conducted. The dynamic deceleration pulse of JAR 25.562(b)(2) must be applied to the fixation point of the tank (for a wing tank this may be taken as the wing root). Structural deformation may take place if this does not result in the liberation of fuel. Single skin baffles and ribs bounded on both side faces by fuel may not be regarded as tank boundaries. Fuel volumes as specified in (i) above must be considered.*

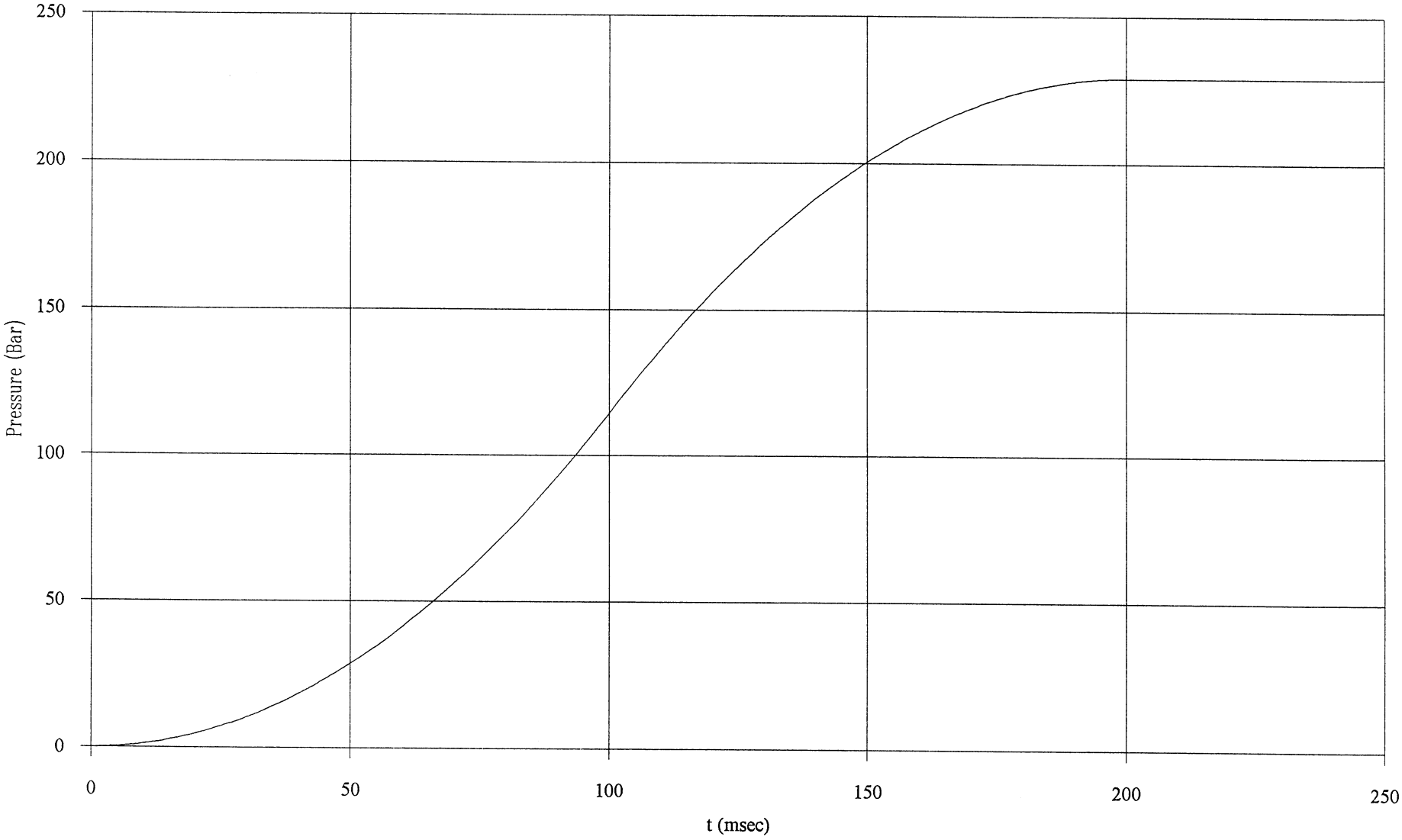

Figure 1 Pressure/time history at the impact face of a long one-dimensional fuel tank subjected to a triangular deceleration pulse. Rise time = 100 msec, peak deceleration = 25g, fuel density = .786gm/cc, bulk modulus = 11100 bar.

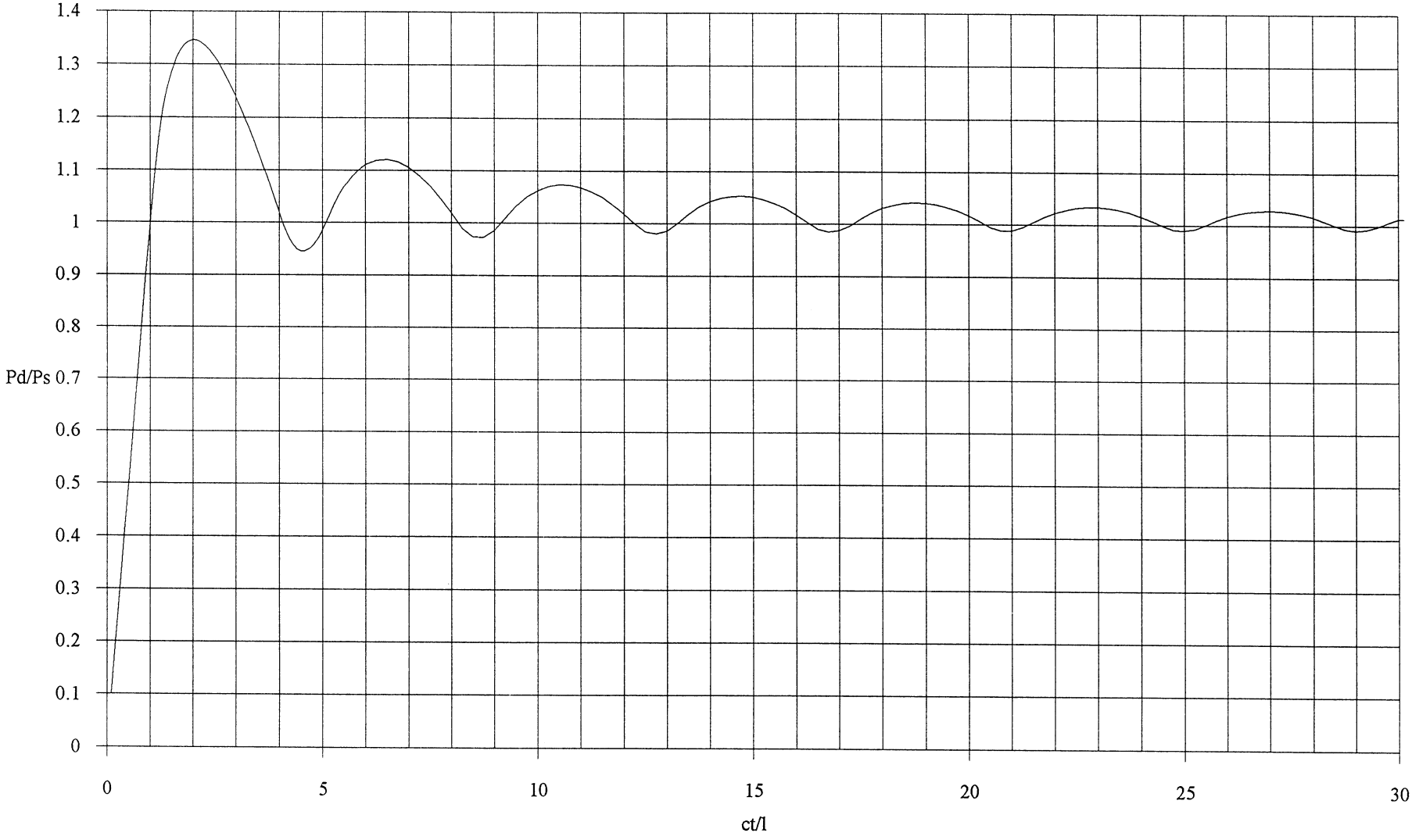

Figure 2 Dynamic pressure determinant from a 25 point finite difference solution for a one-dimensional finite length tank

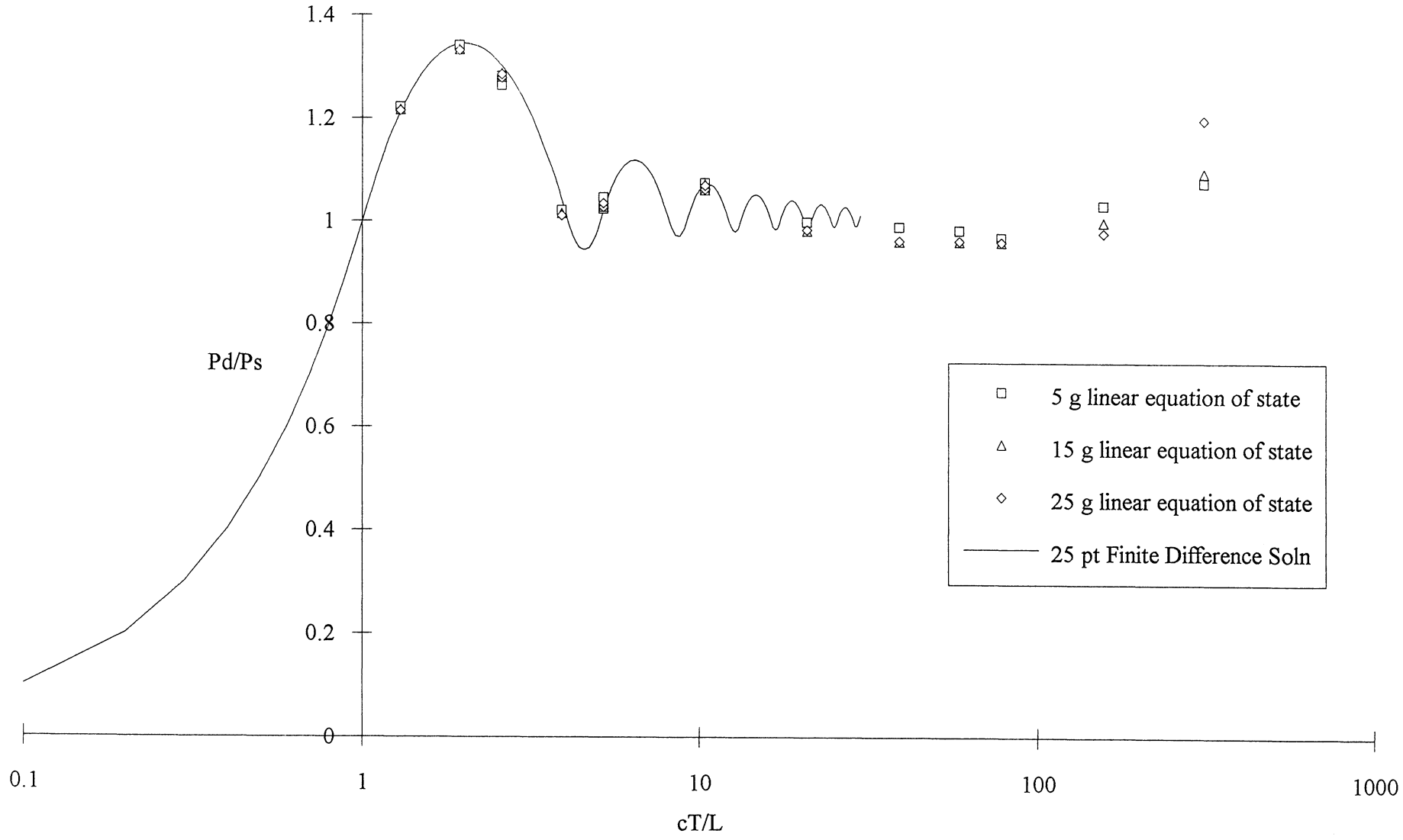

Figure 3 Sowerby Research Centre results. Linear equation of state solutions compared with finite difference derived determinant. (5 ft long tank)

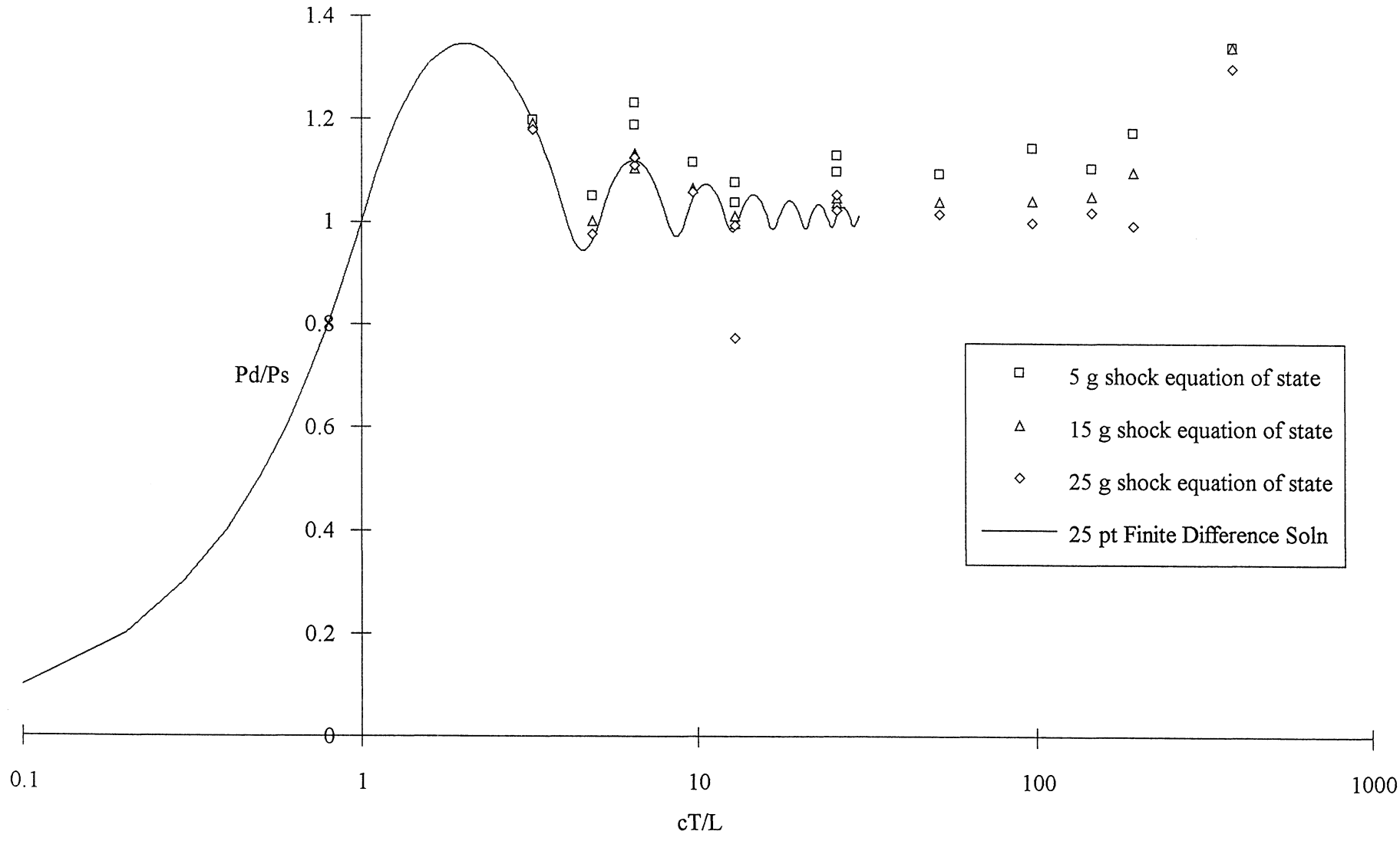

Figure 4 **Sowerby Research Centre results. Shock equation of state solutions compared with finite difference derived determinant. (5 ft long tank)**

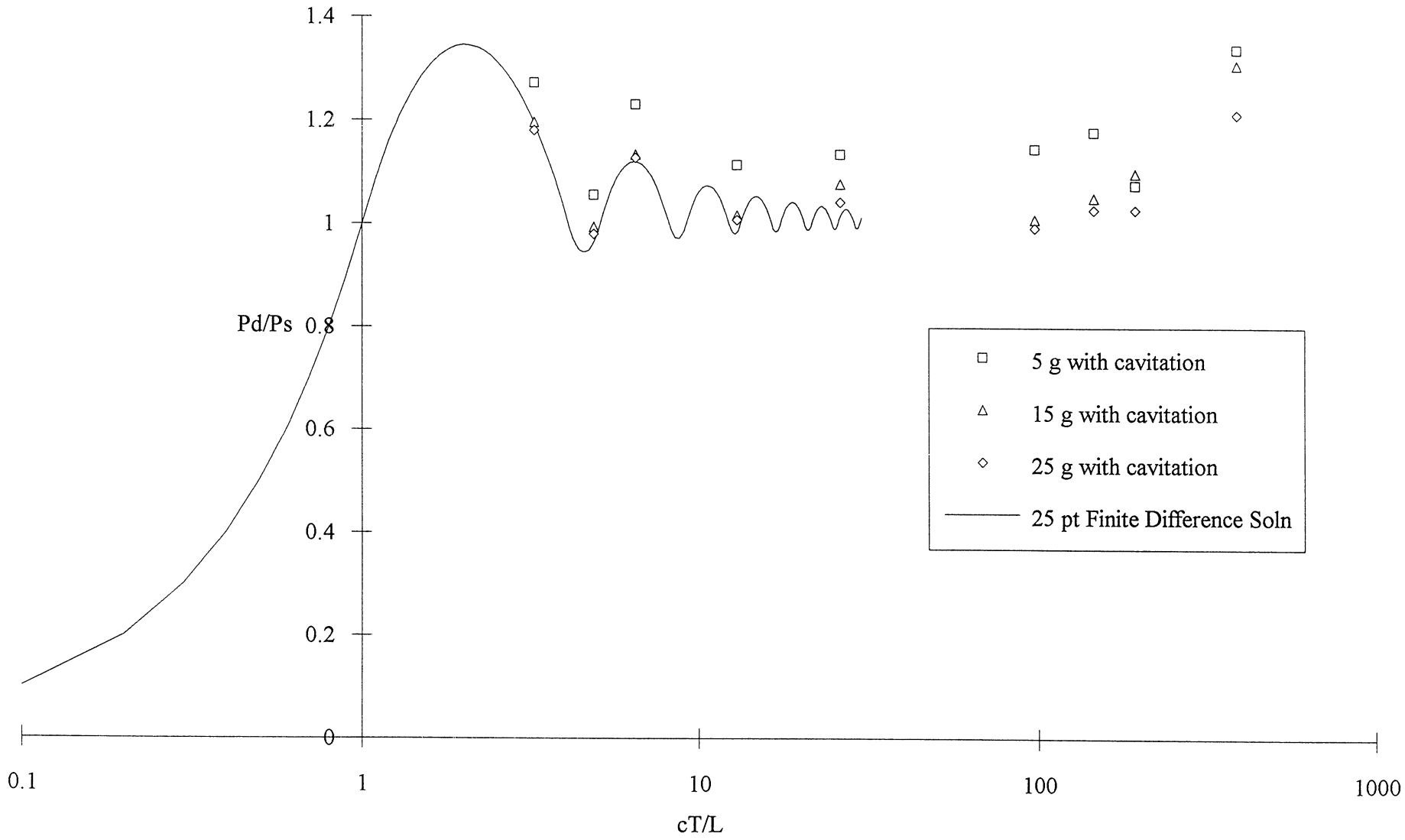

Figure 5 Sowerby Research Centre results. Linear equation of state solutions incorporating cavitation. (5 ft long tank)

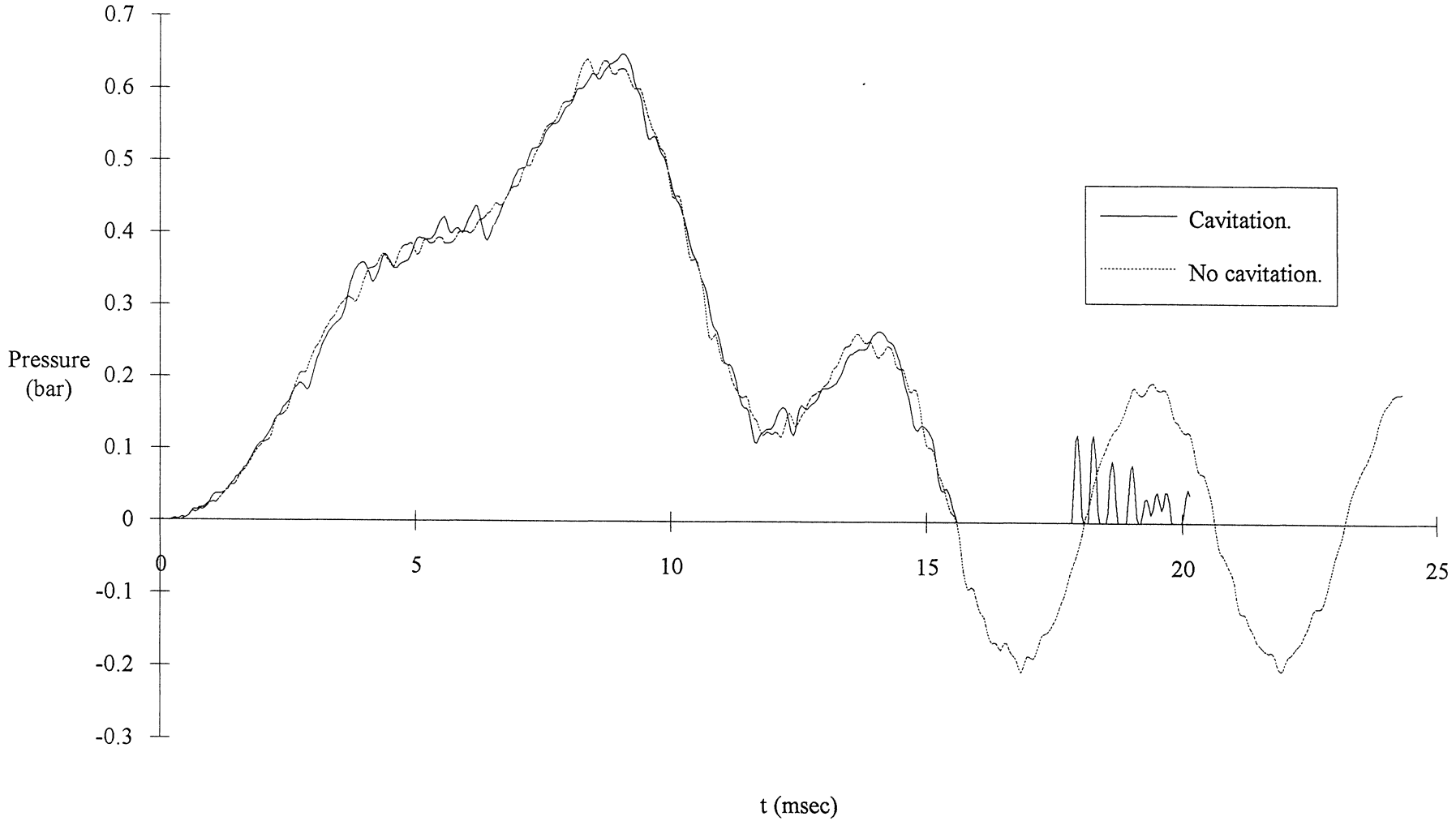

Figure 6 Pressure time history for a 5 ft long one-dimensional tank at the impact face illustrating the effects of cavitation. 5 g deceleration, cT/l=6, JET A1 fuel characteristics

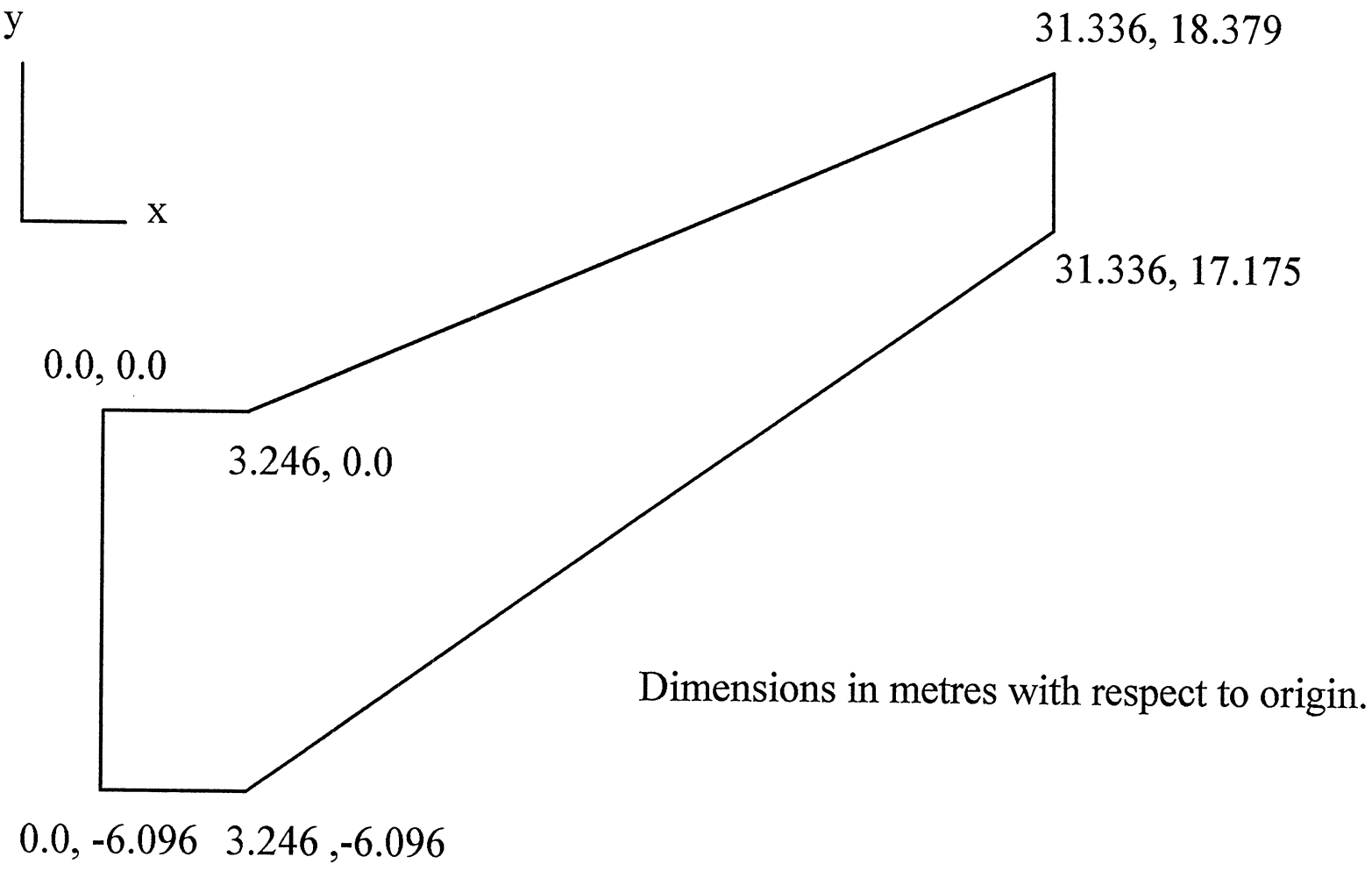

Figure 7 Geometry of 747–400 wing tank used in Sowerby two-dimensional modelling

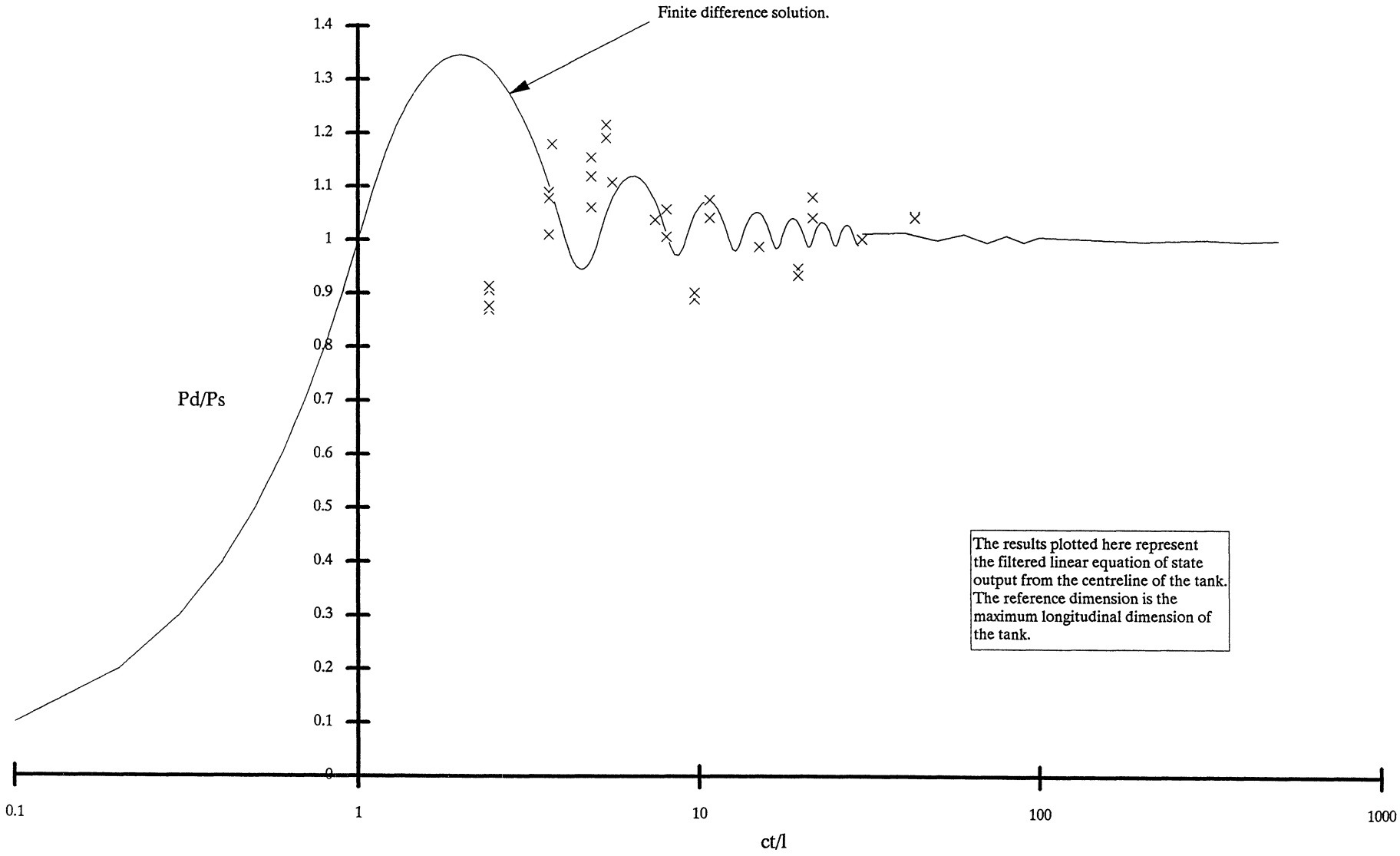

Figure 8 Comparison of 2D analysis with 1D finite difference solution

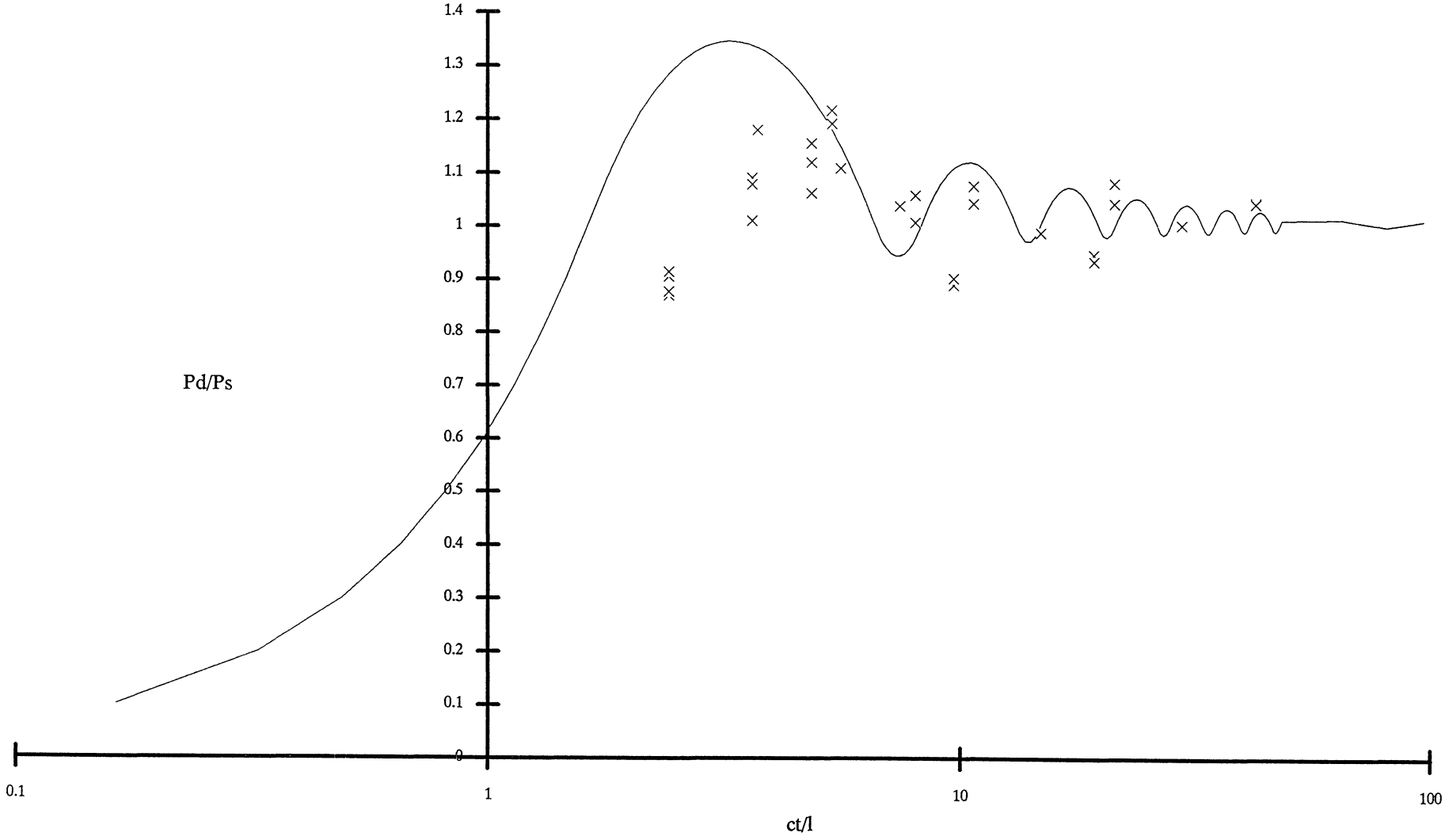

Figure 9 Comparison of 2D analysis with 1D finite difference solution. One dimensional determinant scaled to maximum possible tank length

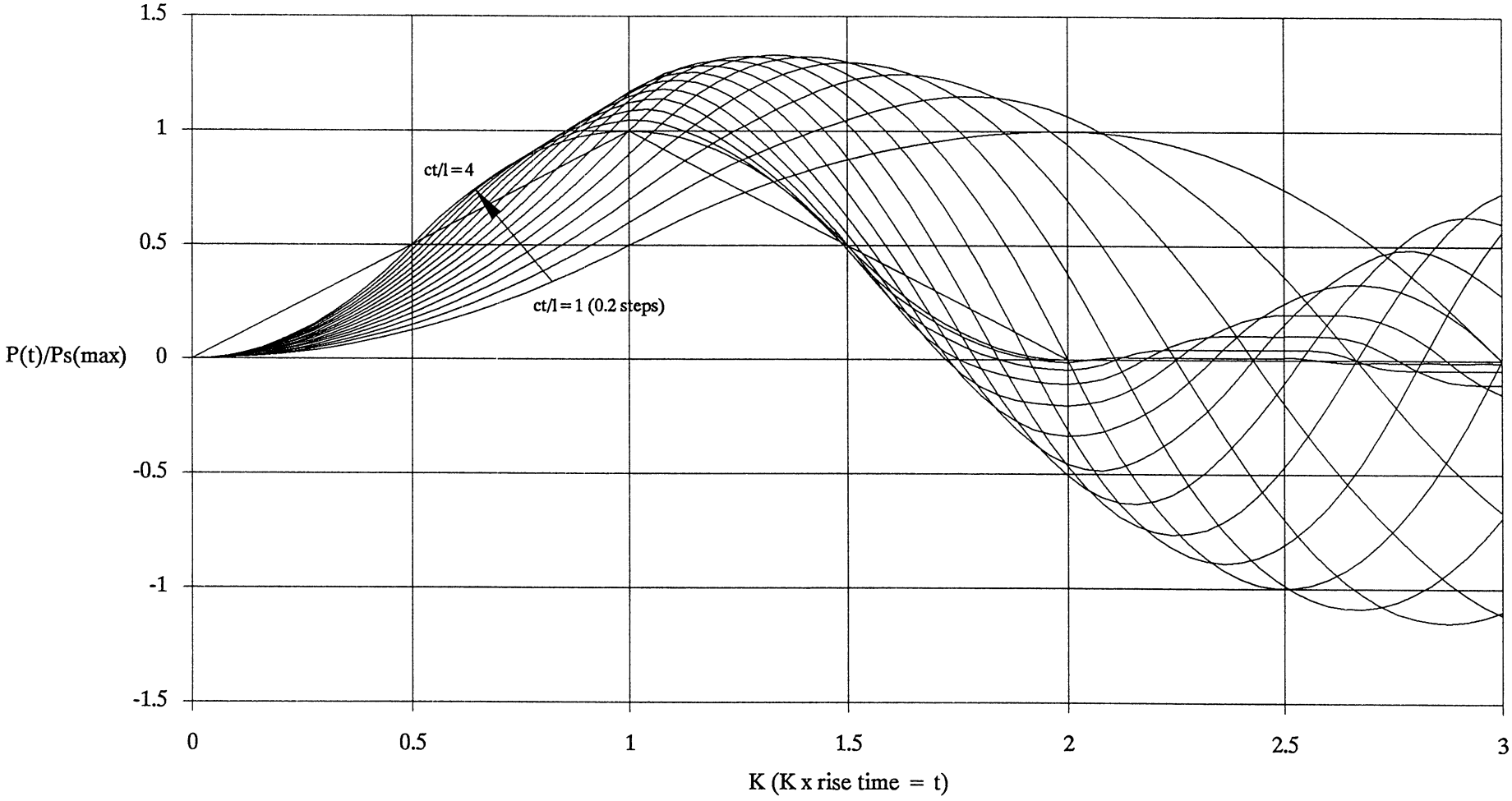

Figure 10 Face pressure pulse shape variation for ct/l = 1 to ct/l = 4

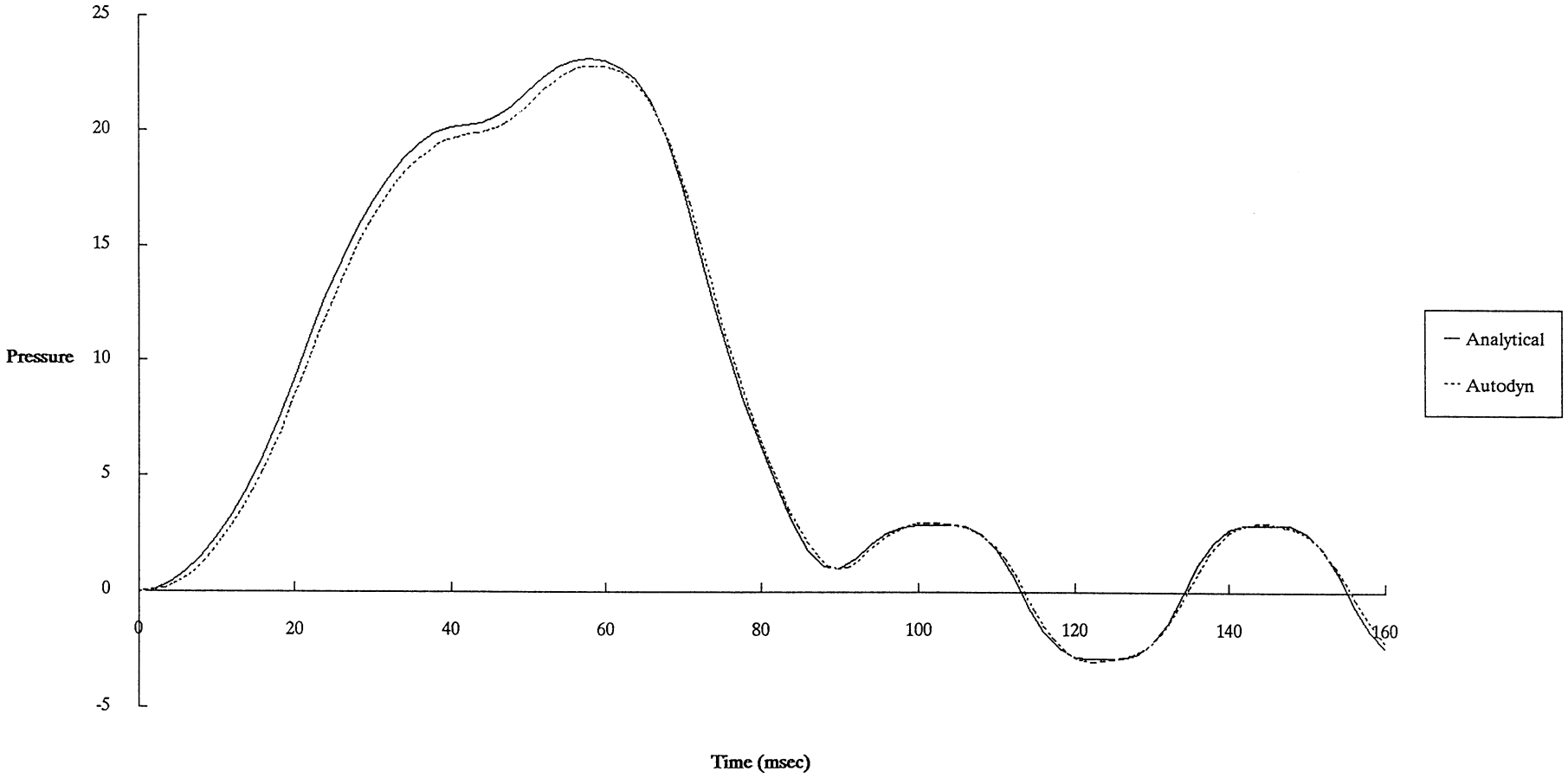

Figure 11 Analytical/Autodyn Comparison 1D 1250cm tank, 50msec rise time, 25g, Jet A1

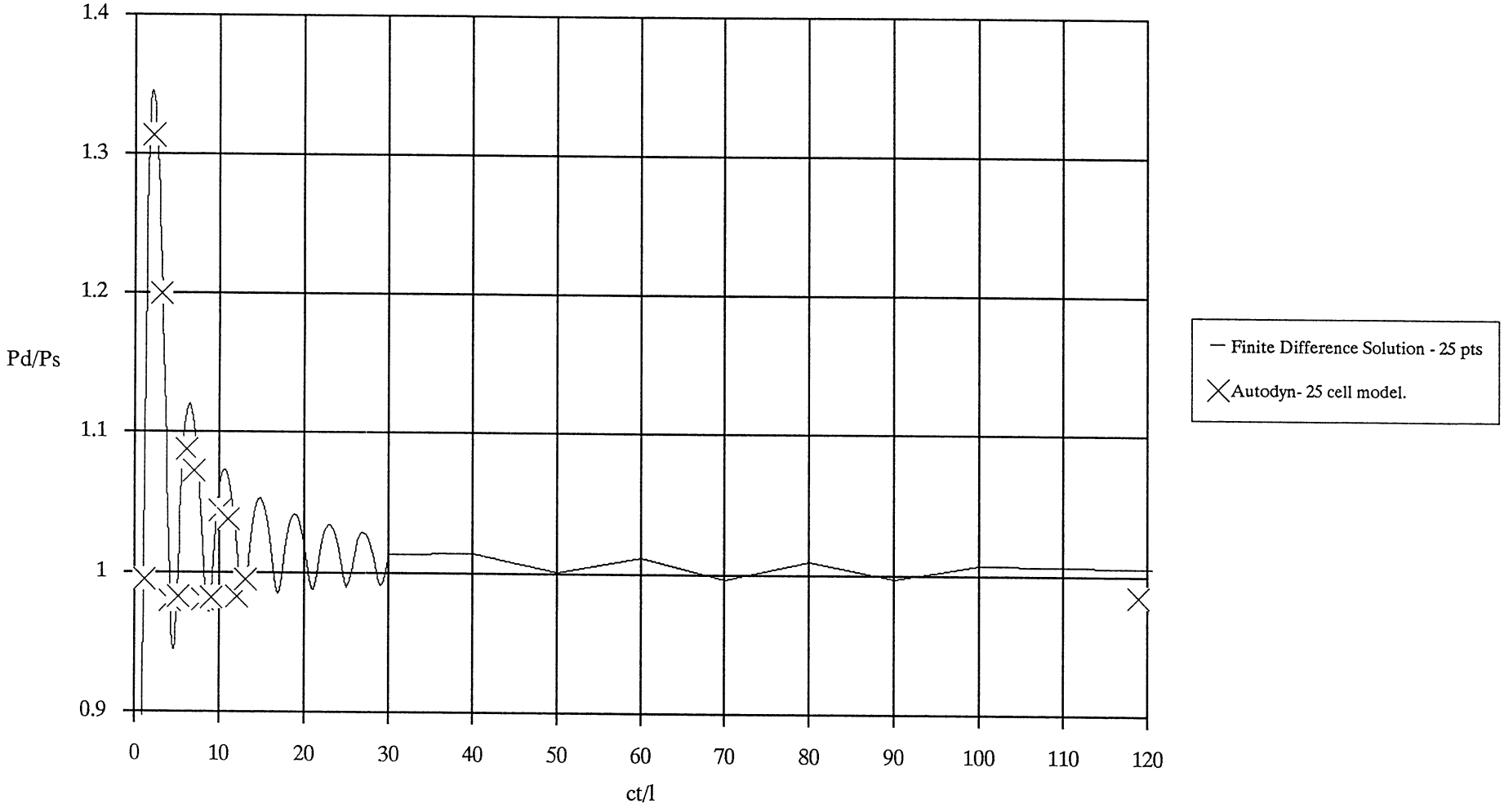

Figure 12 Autodyn-Finite Difference comparison

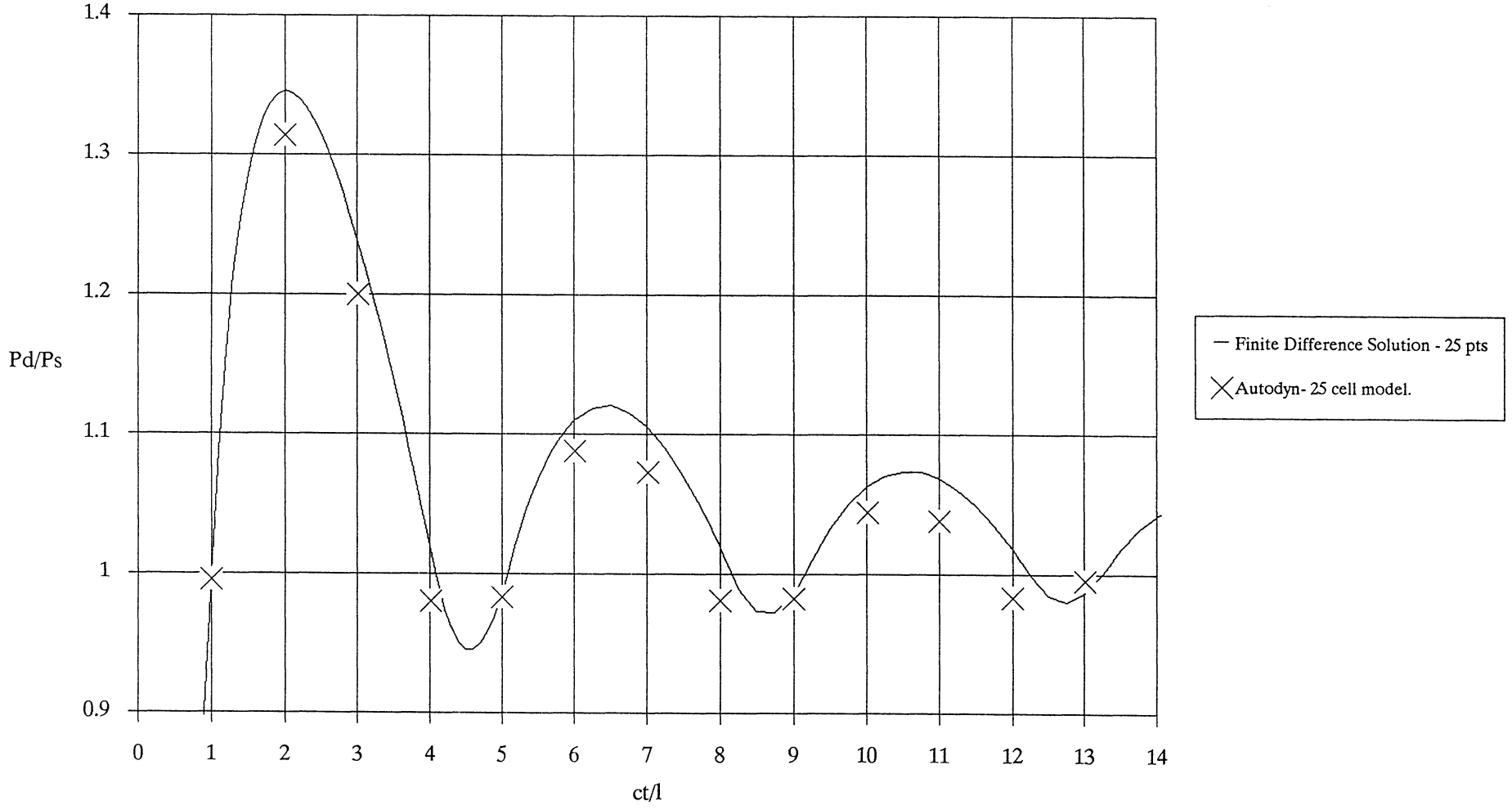

Figure 13 Autodyn-Finite Difference comparison

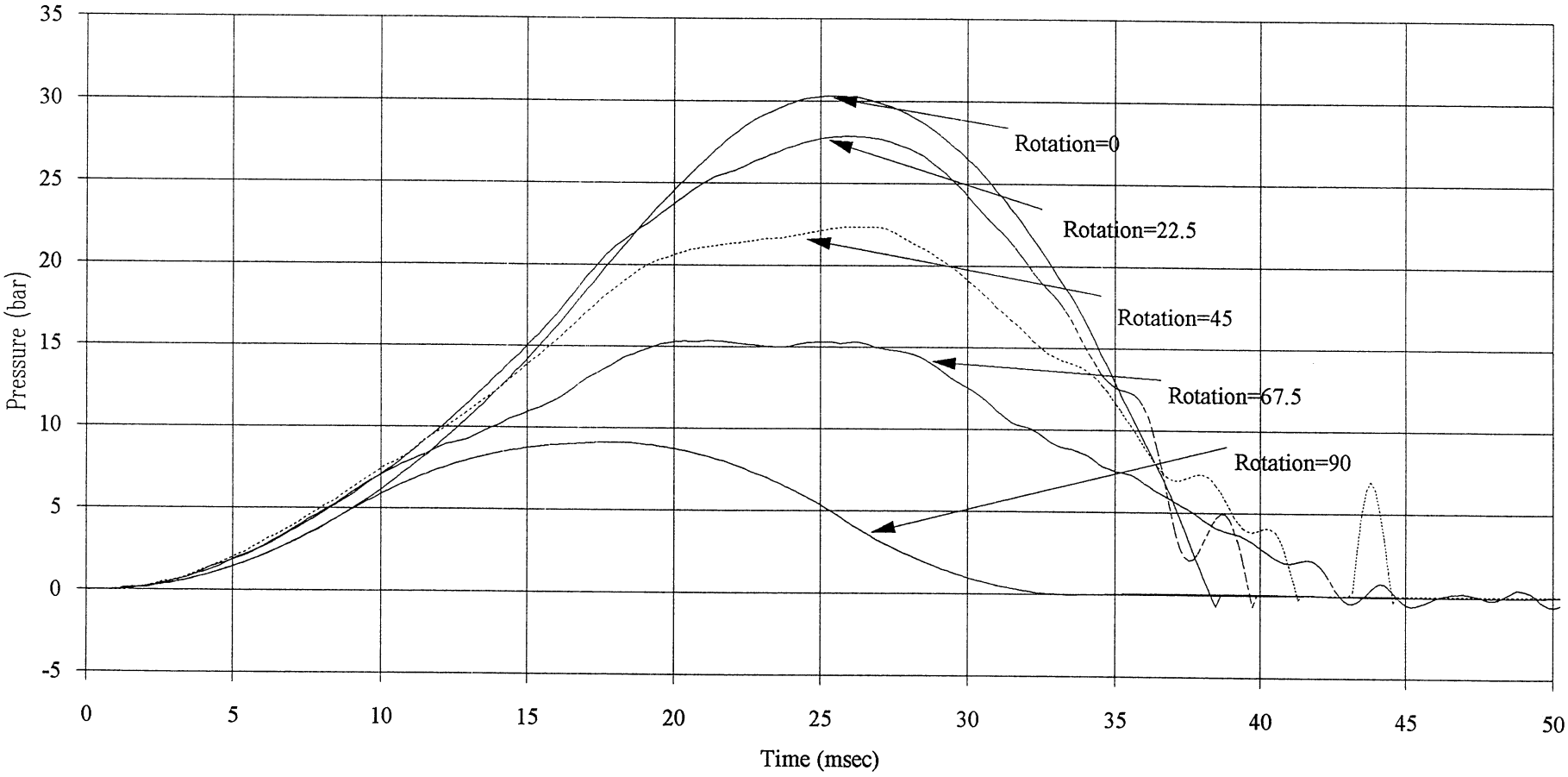

Figure 14 Progressively rotated rectangular tank. 1250cm X 500cm, 17msec pulse rise time, Jet A1, rigid walls. Rotation = 0 corresponds to acceleration parallel to major axis of tank

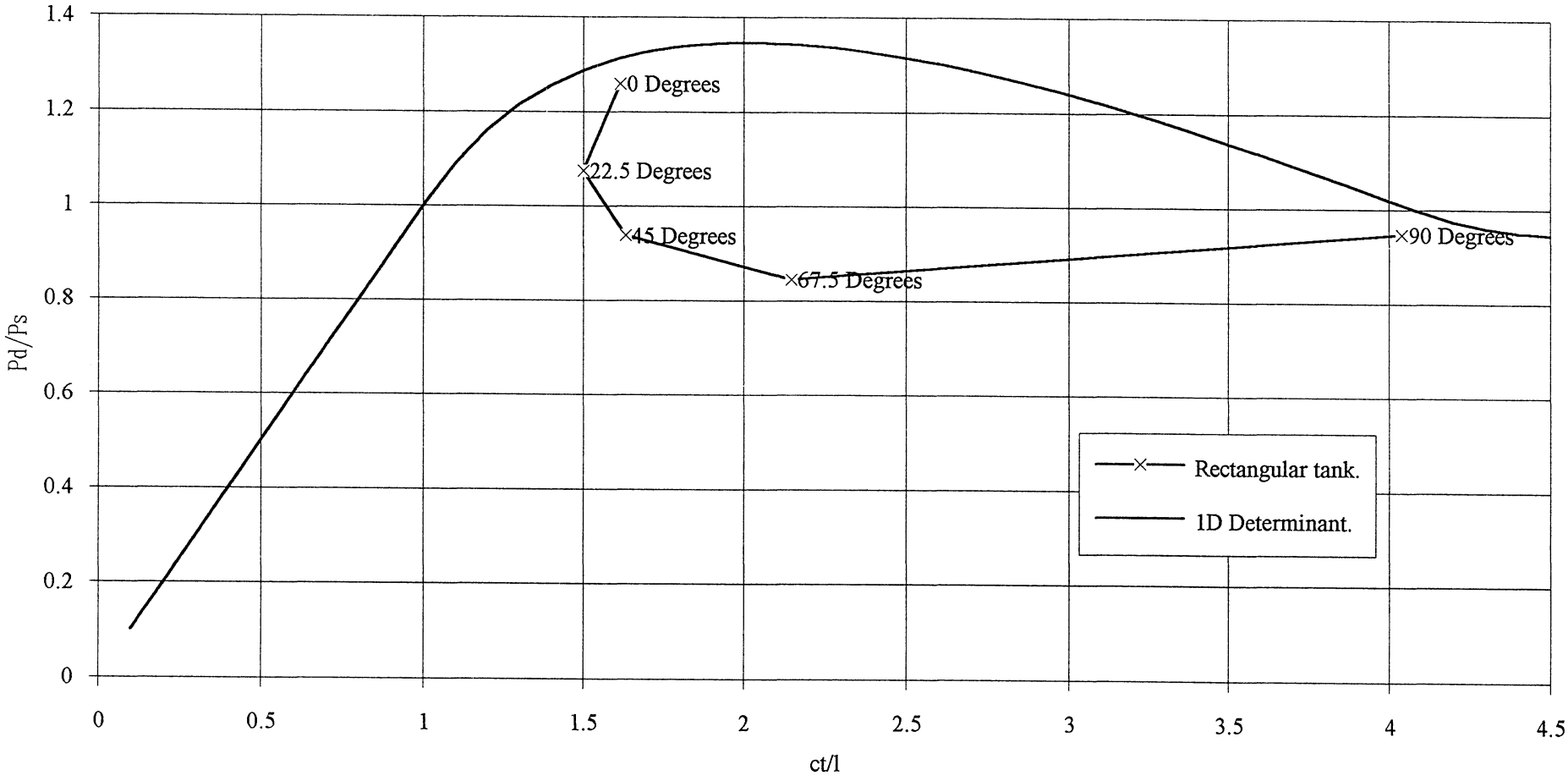

Figure 15 Comparison of response of a progressively rotated rectangular tank with the one-dimensional response determinant

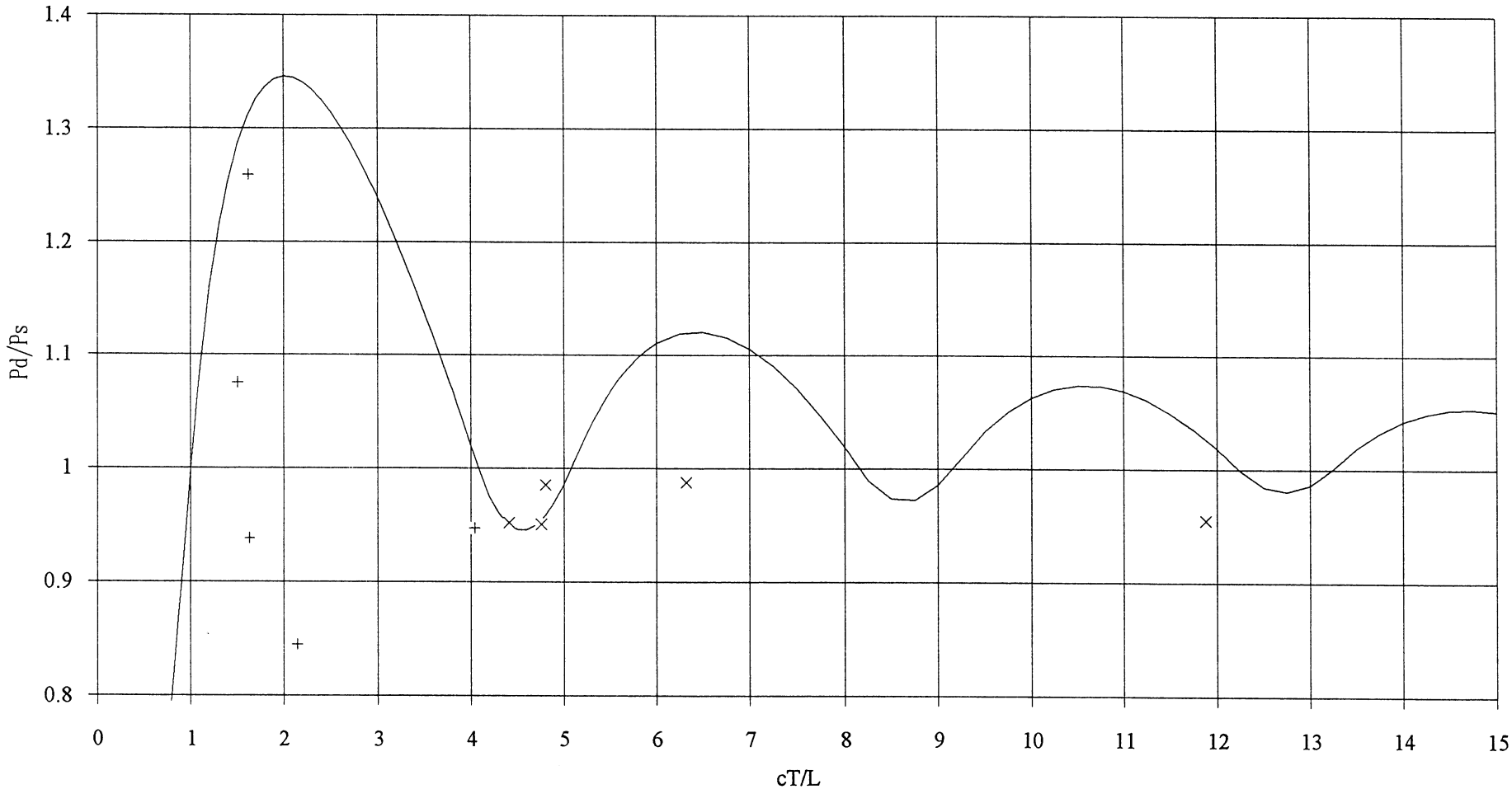

Figure 16 Pd/Ps (max) for a progressively rotated 1250cm x 500cm tank. Comparison with Pd/Ps determinant

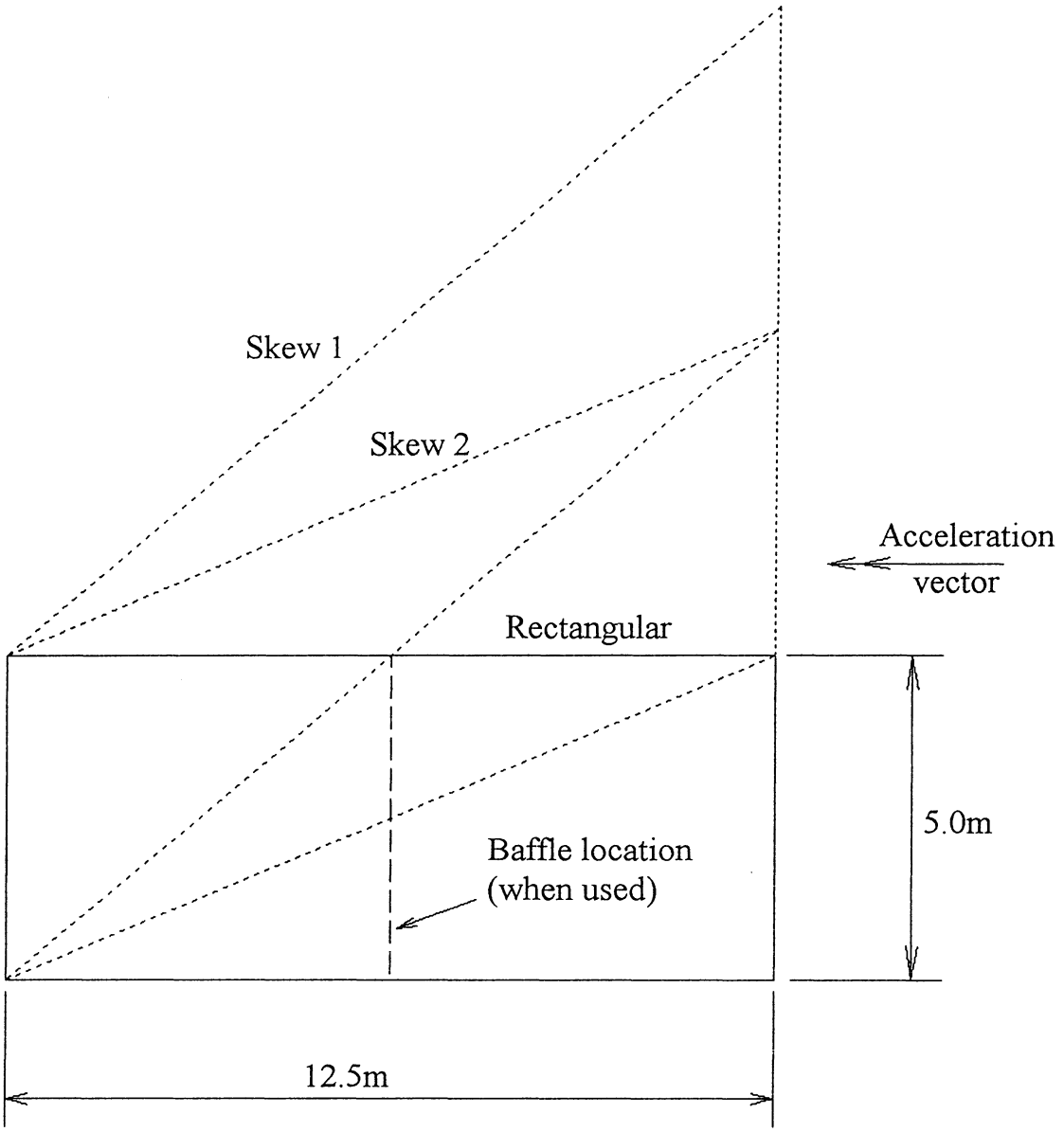

Basic Rectangular 2D Tank.
Skewed tank planforms shown dotted.

Figure 17 Basic Rectangular 2D Tank (Geometry)

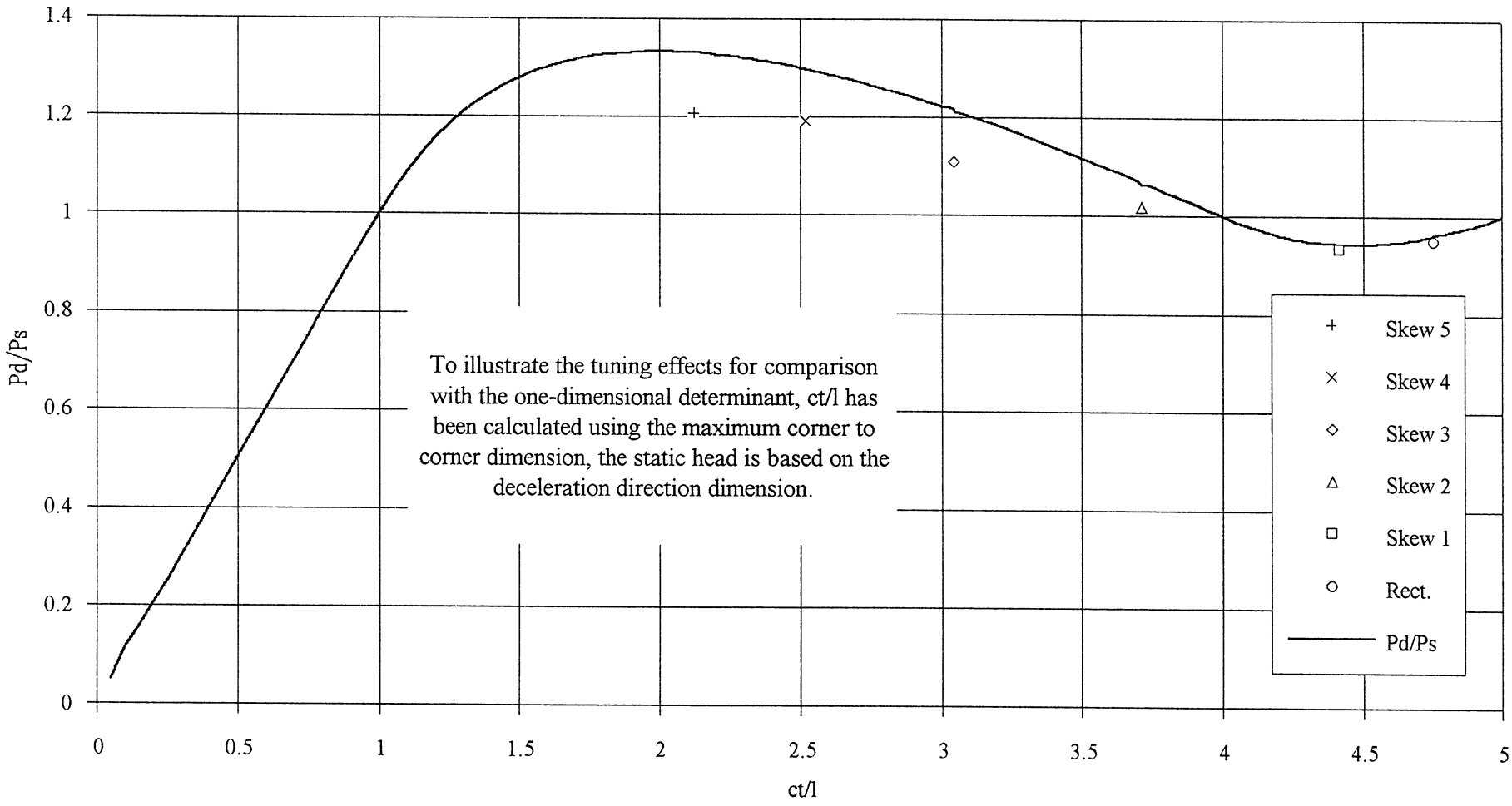

Figure 18 Effect of lateral skew on the pressure response of an initially rectangular tank. Comparison of non-dimensional results with analytical determinant

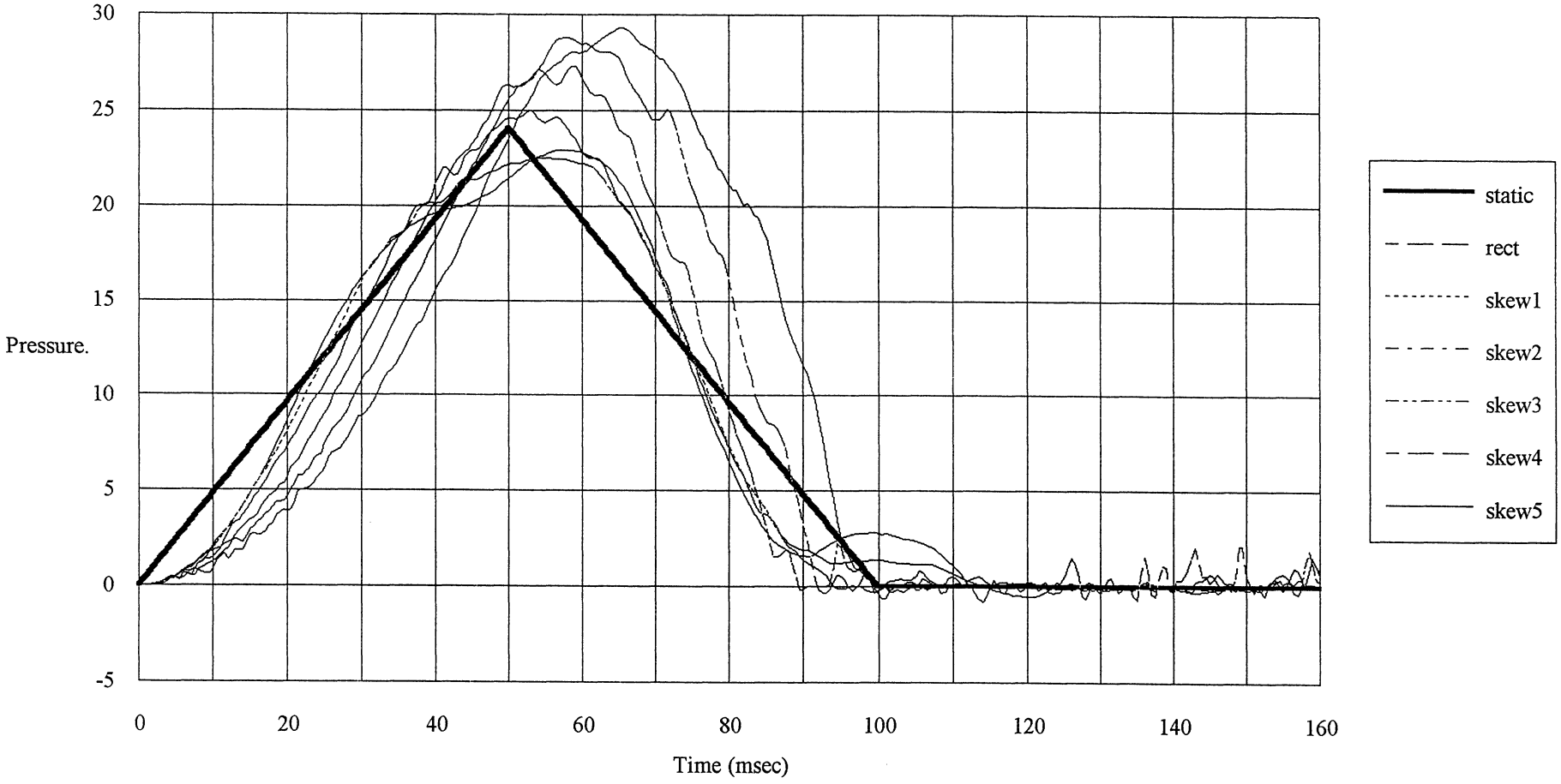

Figure 19 Pressure-Time history for a range of progressively skewed tanks. 25g pulse, 50msec rise time

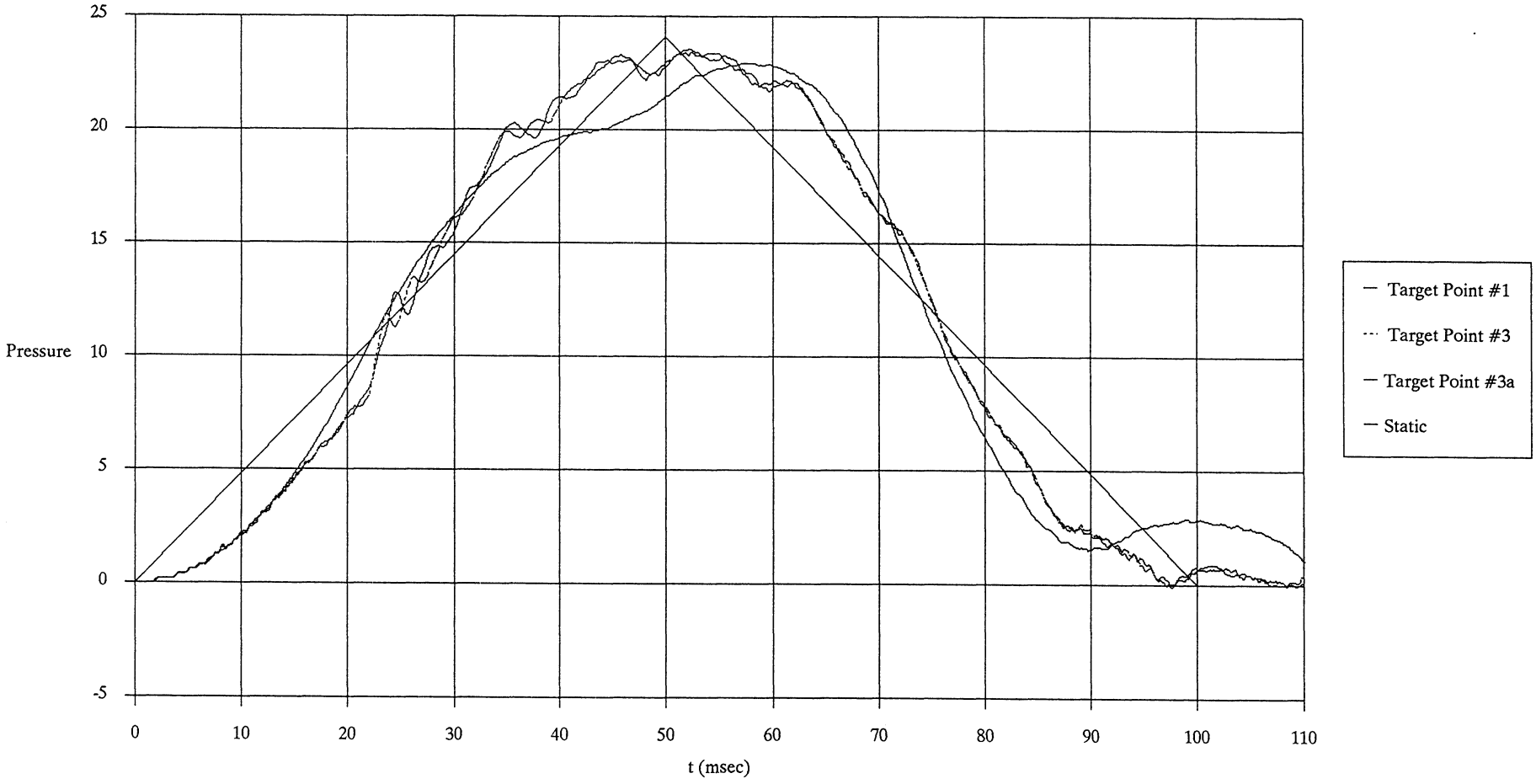

Figure 20 Impact Face Pressure History. Target points 1&3; tank with rigid vented baffle. (T1 at edge, T3 at centre) Target 3a; tank of identical geometry without baffle

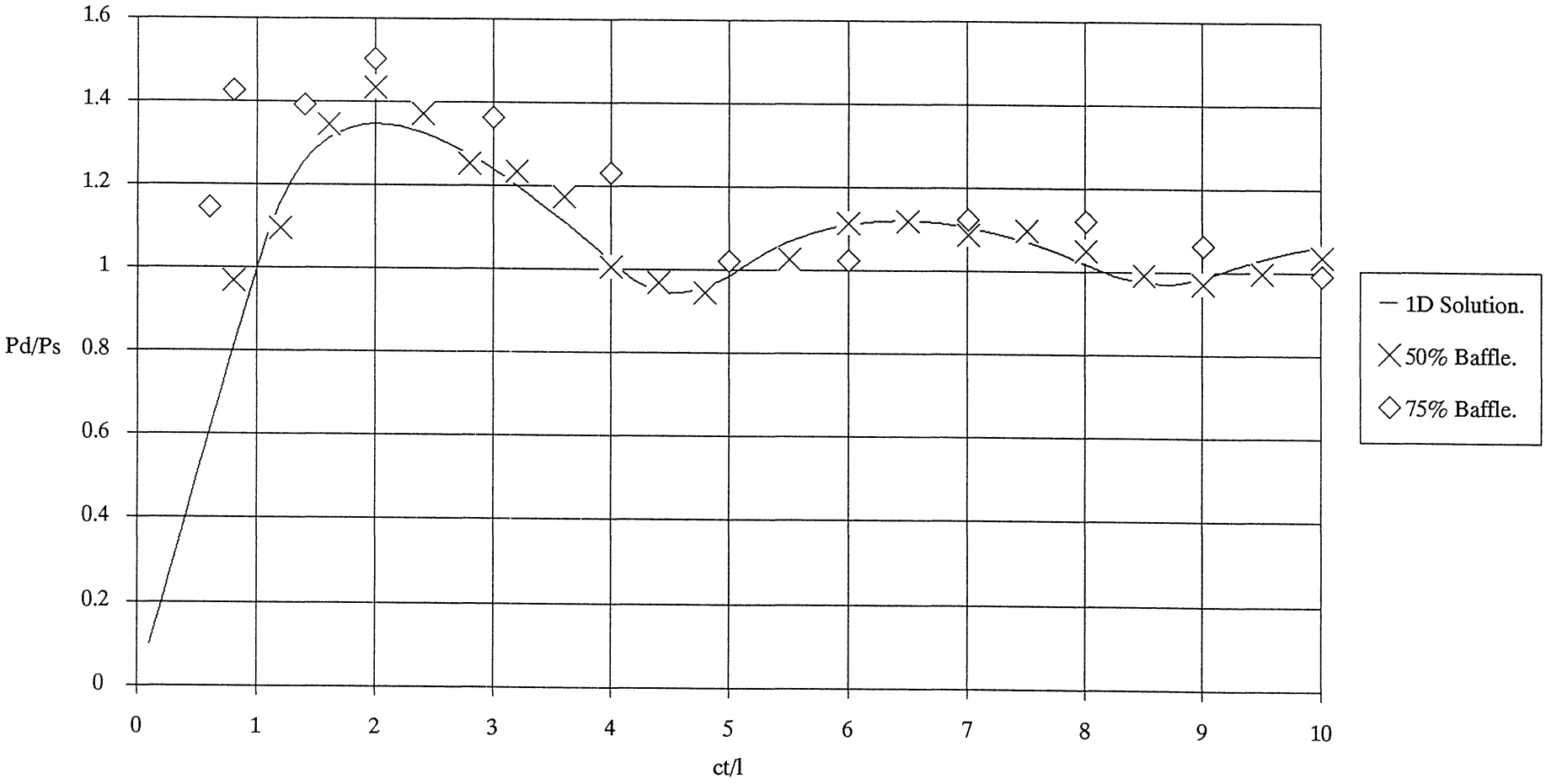

Figure 21 Result of autodyn calculations for a 1250cm long rectangular tank with a segmented baffle at the mid point. Comparison with the Pd/Ps determinant for a one-dimensional un-baffled tank

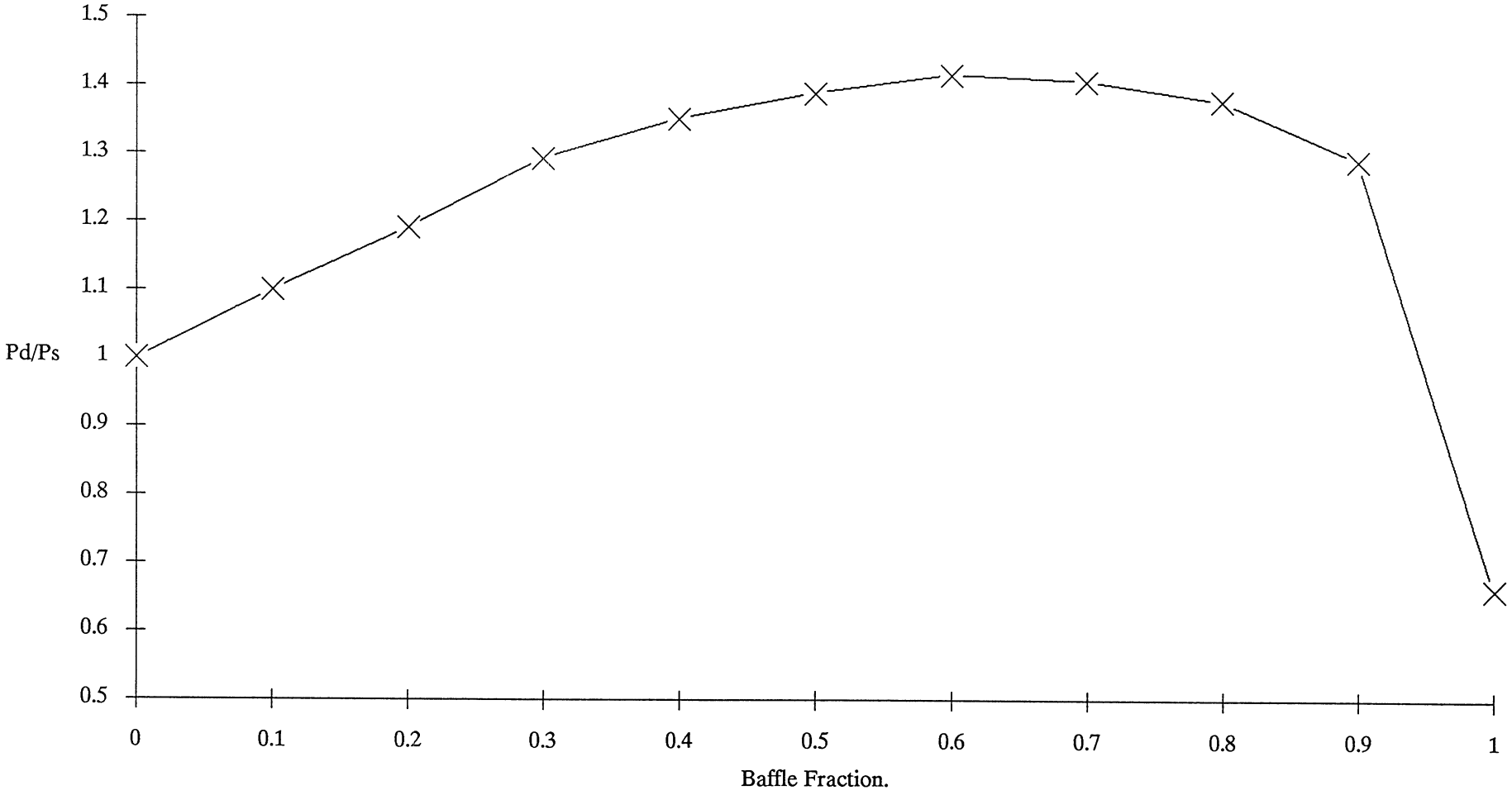

Figure 22 Variation of Pd/Ps ratio with baffle fraction for a simple rectangular tank with a single finely segmented transverse central baffle. ct/l = 1

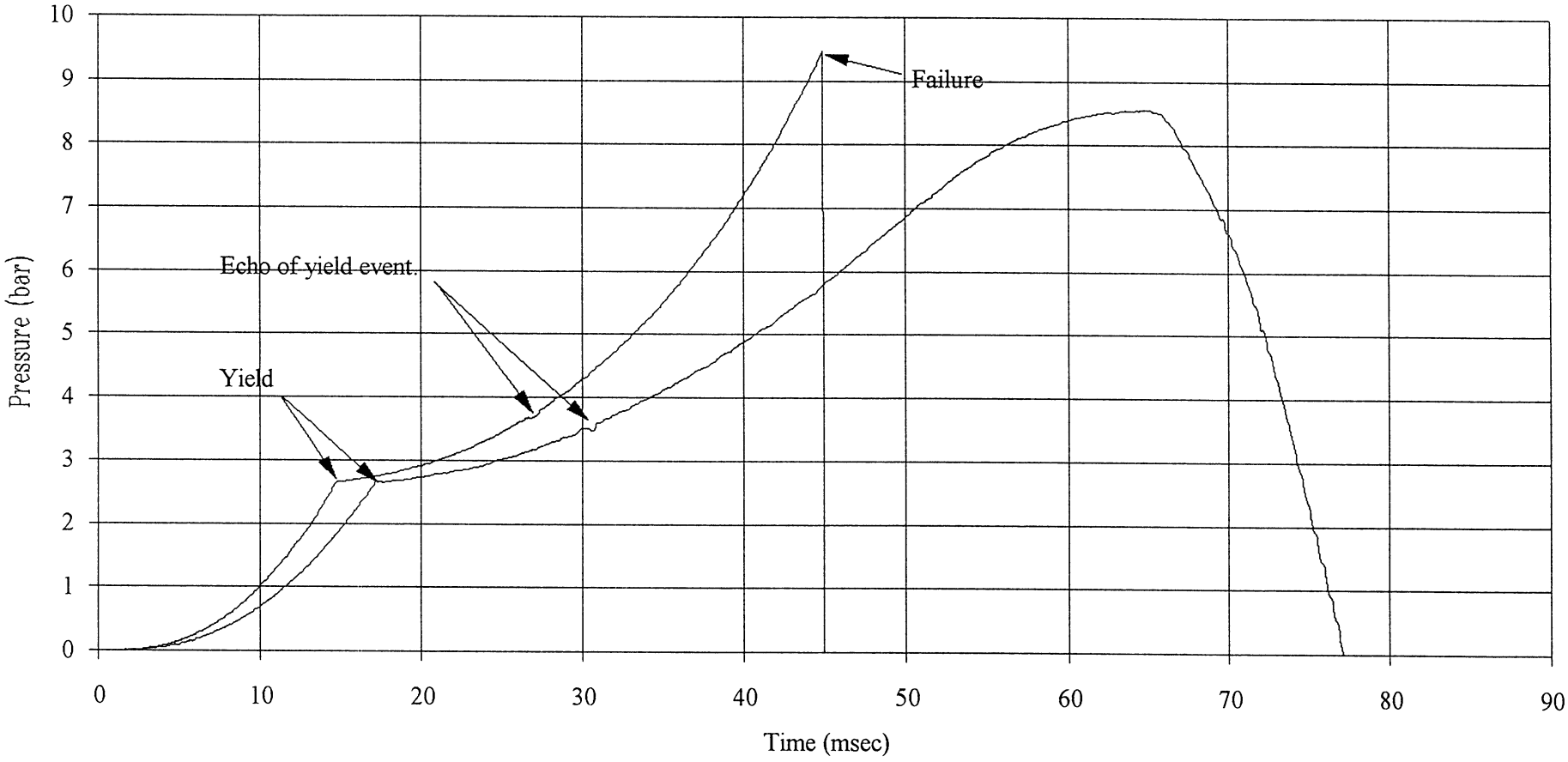

Figure 23 Flexible face 1D tank 30msec rise time. Peak deceleration levels selected to illustrate failure and non-failure of tank. Material failure pressure = 9.065 bar

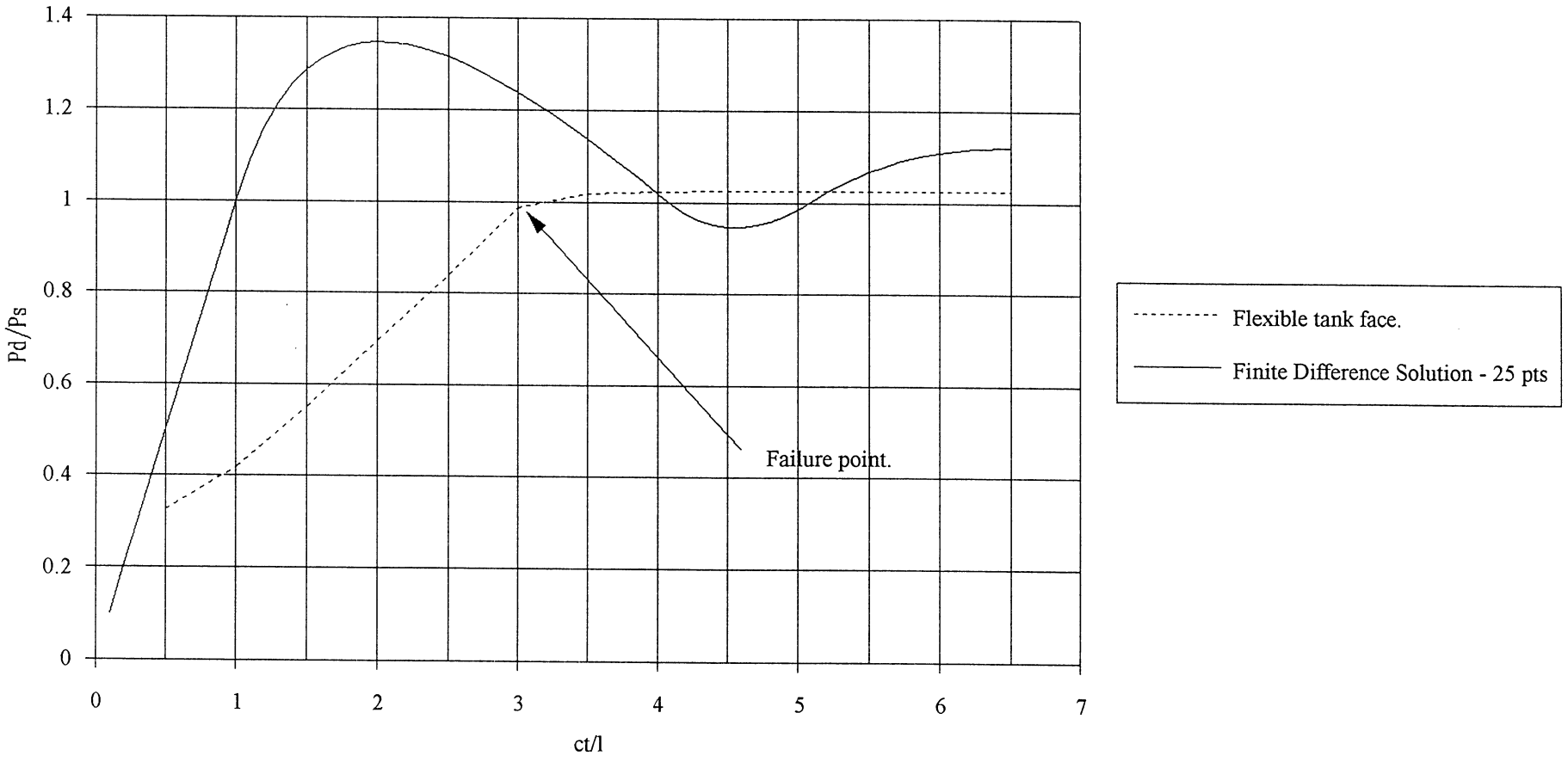

Figure 24 One-dimensional flexible faced tank model. Peak acceleration level sufficient to just cause failure under static head conditions. 1250cm tank, elastic/plastic/failure material model for tank face

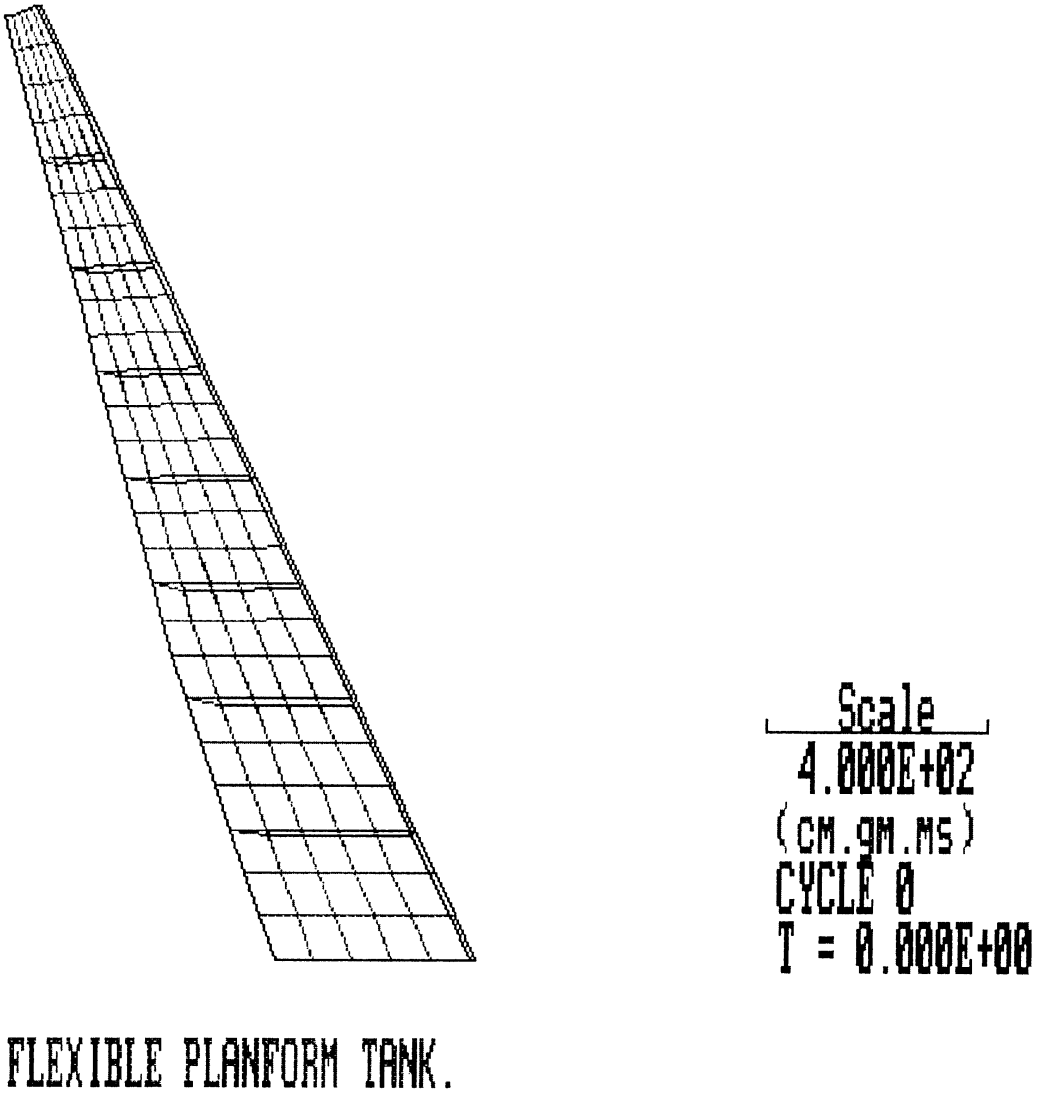

Figure 25 Flexible planform tank (Autodyn model)

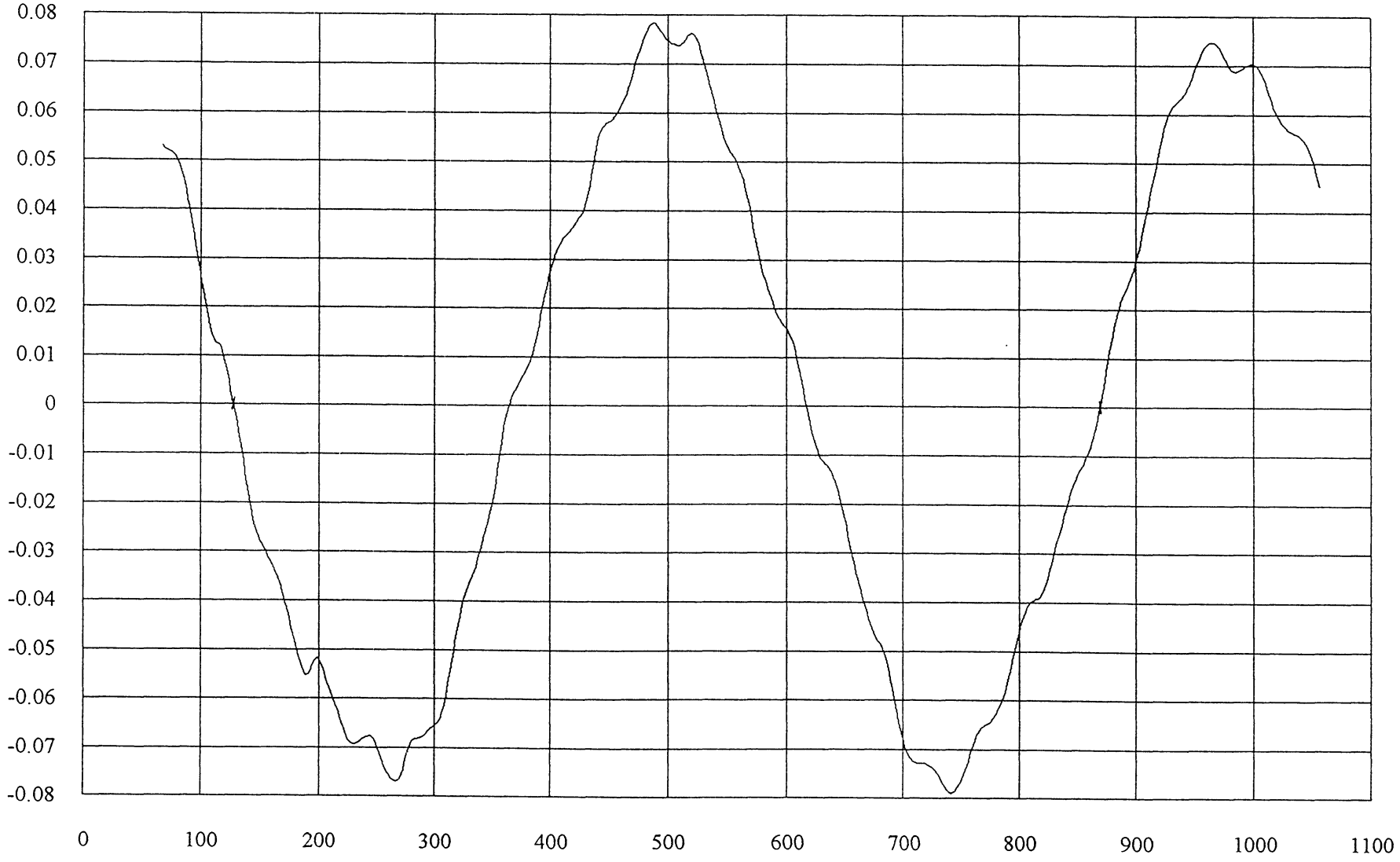

Figure 26 Fundamental fore and aft bending response of planform tank

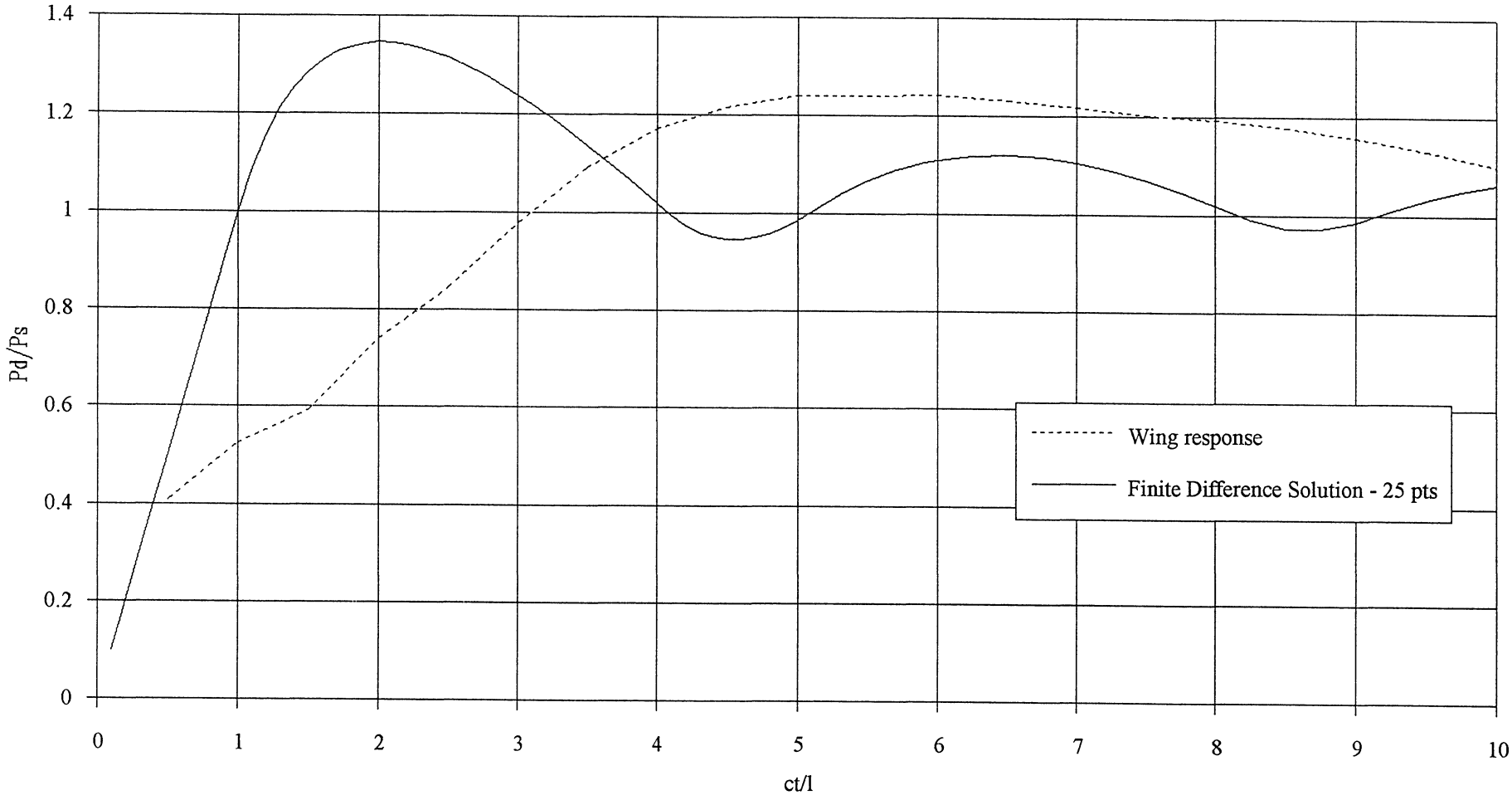

Figure 27 Response of two-dimensional wing planform tank with in-plane bending flexibility for a 16g pulse of varying duration

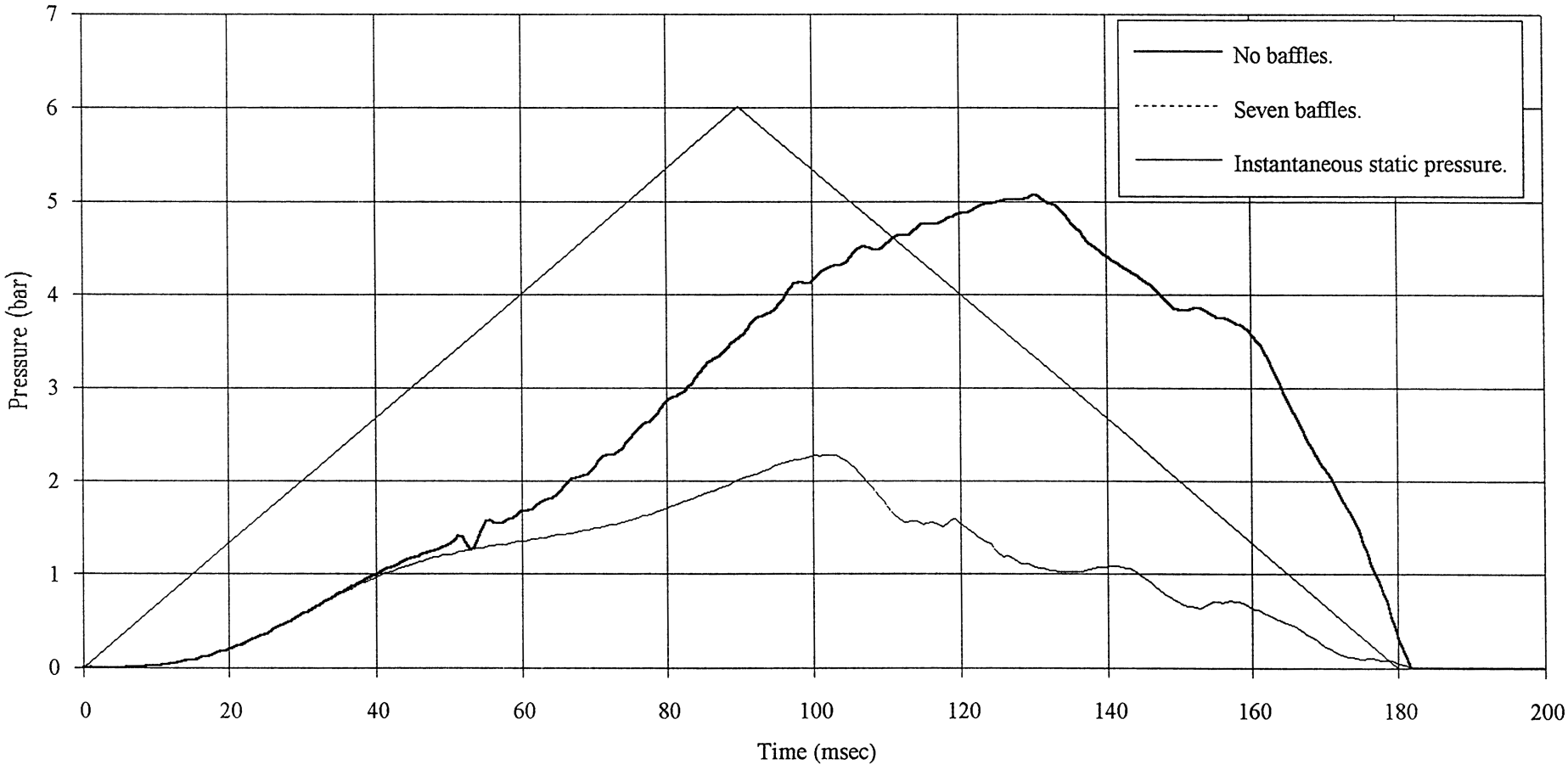

Figure 28 Two dimensional planform wingtank. 9g, 90msec rise time, flexible leading edge structure, wing tuned to a longitudinal bending frequency of 2Hz, flexible baffles

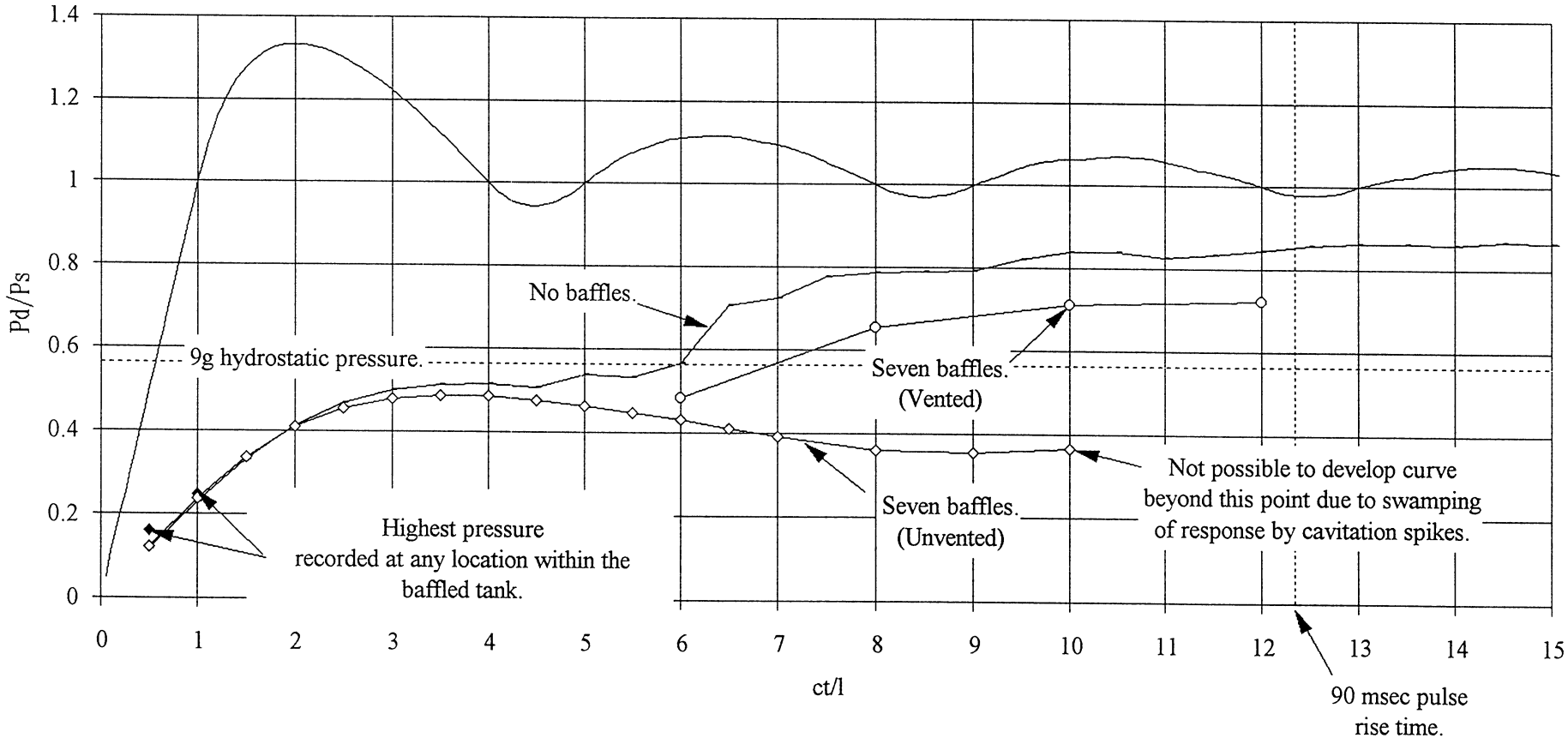

Figure 29 Wing tank (approximate 757 planform). Pressure determinant at tank root unless otherwise stated. Wing tuned to 2Hz in plane bending frequency. Effect of flexible spar web and flexible web plus seven flexible chordwise baffles. 16g peak deceleration

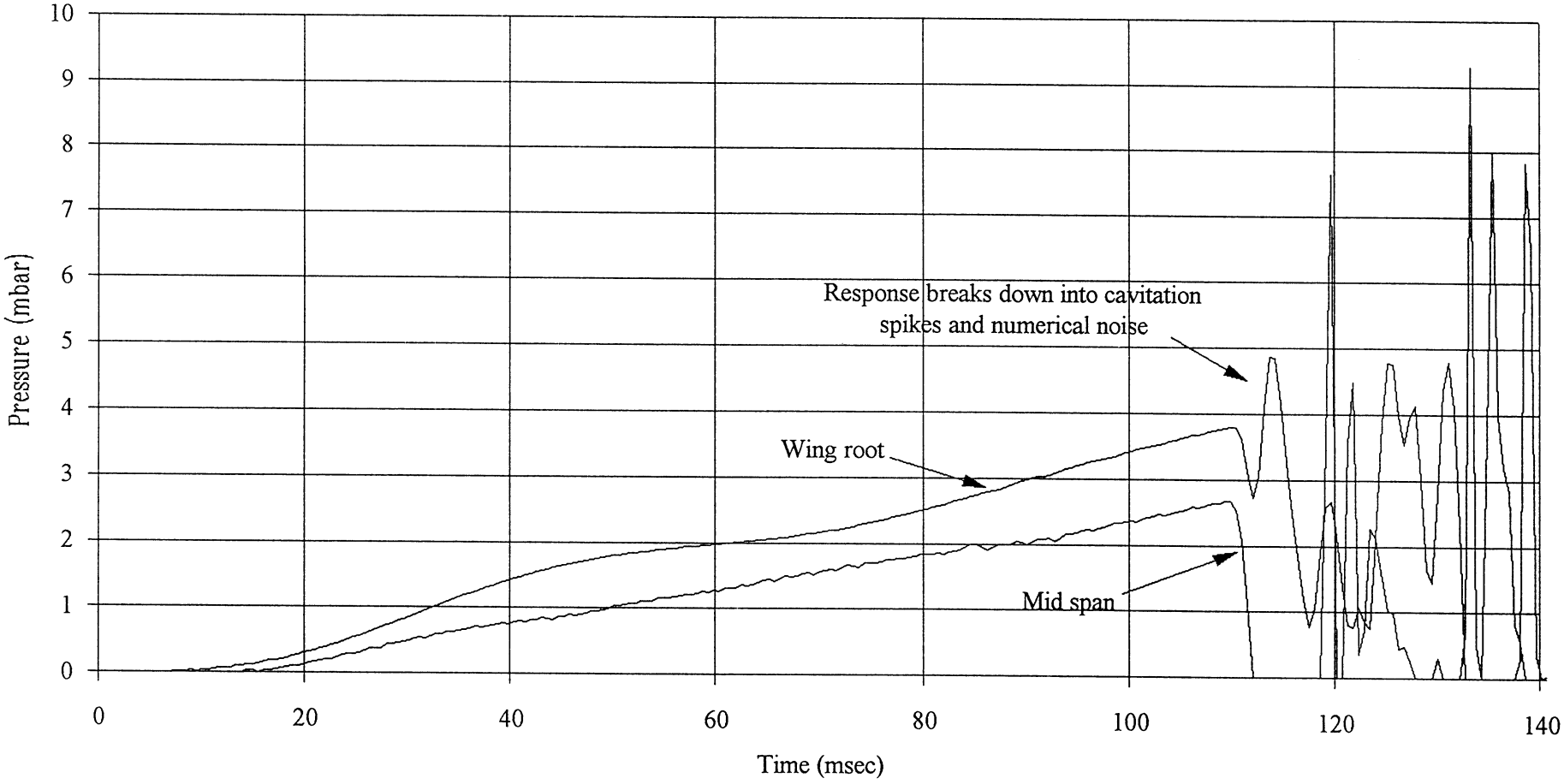

Figure 30 Pressure-time history for a two dimensional flexible walled wing tank with seven chordwise baffles. Ct/l = 15, pulse rise time = 109.4msec